Applications of Finite Element Modeling (FEM) and Experiments to Study the Mk1 PB-FHR Center Reflector

NE 170 – Senior Design Project

Brigette Badro, Cameron Bailey, Stephen Kaplan, Hin Lee, and Mariam Malek
Department of Nuclear Engineering
University of California, Berkeley

Report UCBTH-14-004

May, 2014

ABSTRACT

In this project, the design team used finite element modeling (FEM) methods to identify areas of peak stress and potential failure points in the internal center reflector of a Mark-1 Pebble-Bed Fluoride Salt Cooled High-Temperature Reactor (Mk1 PB-FHR) due to neutron irradiation damage. The FEM modeling examined design options to reduce these peak stresses, including axial and circumferential segmentation of the reflector blocks. The team also studied the stability the center column to buckling during seismic events. The team subsequently performed static push-over tests and shake tests to observe the behavior of the individual graphite blocks of the center at different magnitudes of seismic events. The static push-over test determined the horizontal where the graphite blocks of the center reflector would unhinge. A simplified analytical model to predict the static push-over force required to cause buckling was developed, and compared to the experimental data.

TABLE OF CONTENTS

1.0 INTRODUCTION

As shown in Figure 1.1, the Mark-1 Pebble-Bed Fluoride Salt Cooled High-Temperature Reactor (Mk1 PB-FHR) uses an annular pebble core with a graphite center reflector that contains channels for control rods and instrument tubes, as well as flow channels to inject coolant along the lower half of the reflector. Fuel and reflector pebbles are fed into the bottom of the annular using 8 feed tubes. The reflector pebbles form a layer outside the fuel pebbles, which shields the outer graphite reflector. The pebbles move slowly up through the annular core region between the center and outer radial reflectors. The pebbles are removed through a defueling slot at the top of the core (Andreades et al., 2014).

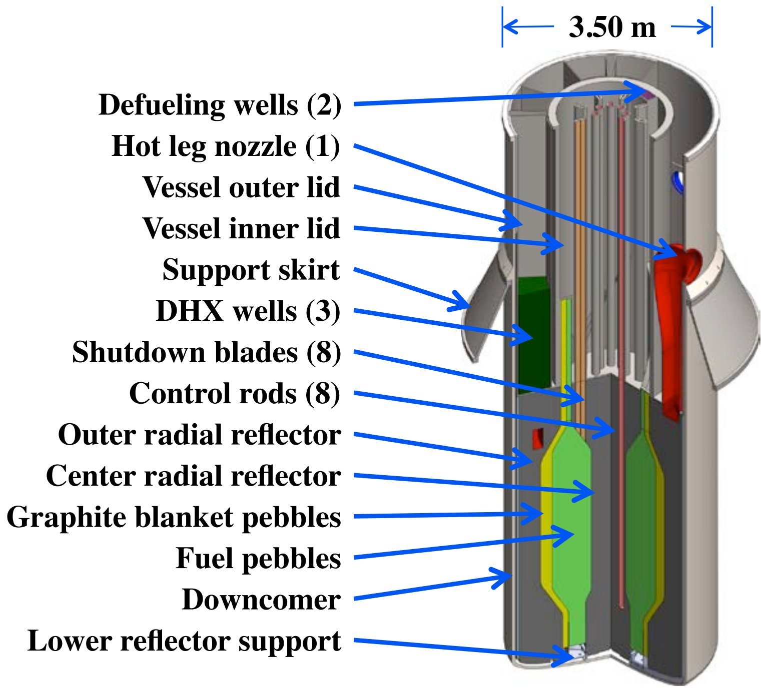

Figure 1.1: The Mk1 reactor design showing the annular pebble core.

The center reflector is exposed to large doses of fast neutrons which cause damage to the graphite. This reflector also must be capable of surviving earthquakes without buckling or failing. This design study focused on the design and modeling of the Mk1 center reflector, and recommends design modifications to further improve its performance.

The study examined stresses induced by neutron irradiation in the current Mk1 design of the center reflector using finite element modeling (FEM). The goal of using FEM was to provide a preliminary estimate for the lifetime and replacement frequency for the center reflector, which must be replaced periodically due to neutron irradiation damage. The estimate provided by this modeling is preliminary, because it did not include modeling of the effects of creep, which would relieve stresses and thus extend the life of the reflector compared to the estimates calculated here.

A key goal of the FEM modeling was to determine how the geometry of the center reflector blocks could be optimized to reduce stresses induced by neutron irradiation damage, and in particular the effects of segmenting the blocks axially and circumferentially. By using FEM methods with the multi-physics code Comsol, areas of peak stress during seismic events were determined (neglecting the effects of creep). Comsol was also used to simulate the effects of neutron damage for the center reflector.

This design study also performed experiments and developed an analytical model to better understand how buckling could occur in the Mk1 center reflector during seismic events. Experiments were conducted for both the static push over force, as well as a shake test. The experiments included a simplified model for the reflector (a stack of cat-food cans) and a wooden model designed to replicate the geometry of the Mk1 center reflector. The also included a static tilting test to determine where and how the blocks would dislodge or unhinge when tilted, creating a static push-over force.

2.0 DESIGN OF THE MK1 CENTER REFLECTOR

The Mk1 design uses an annular pebble core geometry. Because the pebbles float, they are fed into the bottom of the core and move slowly upward, to be removed through an annular defueling slot at the top of the core by tow defueling machines. The Mk1 core uses a simplified pebble core comprised of a homogenous mix of fuel pebbles adjacent to the center graphite reflector, with a layer of inert graphite reflector pebbles on the outside that reduces the fast neutron fluence to the outer fixes radial graphite reflector sufficiently for it to last the life of the plant.

The center graphite reflector, shown in Figure 2.1, is much shorter and smaller than center reflectors that have been designed for helium cooled pebble bed reactors, simplifying its design for replacement and for seismic qualification. The center reflector provides 8 channels for insertion of buoyant control rods and it also provides flow channels for radial injection of coolant into the pebble core to provide a combined radial and axial flow distribution that increases the effectiveness of heat transfer from the fuel and results in lower average fuel temperature.

The blocks in the center reflector in the PB-FHR are designed so they can be machined using a multi-axis computer numerically controlled (CNC) milling machine. The geometry of the center reflector blocks contain no reentrant features, and can be machined with a multi-axis CNC milling machine using only plunging motions.

The center reflector performs multiple functions. Because it receives high neutron dose, it is designed to be replaceable as a modular unit. It is designed to be fabricated from 0.26-m thick graphite billets, which are machined to a net thickness of 0.25 m to provide keys that maintain the vertical alignment of the reflector blocks. One of the goals of this project was to study how neutron-irradiation induced stress varies when the block height is changed.

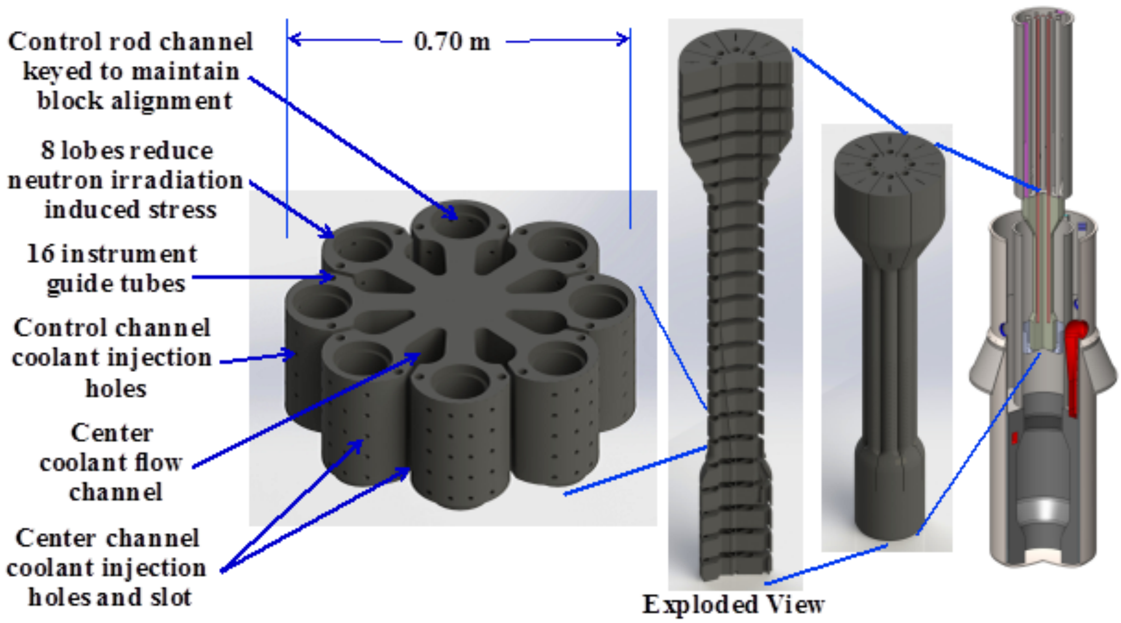

Figure 2.1: Replaceable Mk1 center graphite reflector

Because the nominal density of the graphite, 1740 kg/m^3, is slightly lower than the density of the primary salt (1963 kg/m^3 at 650°C), these blocks are nearly neutrally buoyant, but float in the primary coolant. Thus the blocks float upward and rest against the metallic center upper core support structure, which is keyed to maintain alignment so that shut down blade and control rod elements can pass through channels machined into the reflector blocks. This means that the top block in the column is restrained both axially and horizontally.

The bottom block in the column is also restrained against horizontal motion by the lower reflector support ring, which transfers horizontal loads into the core barrel. However, because the core barrel and the center reflector column have different axial thermal expansion, this bottom support does not restrain the bottom block vertically, and instead the block floats up against the blocks above it. It is not possible for the blocks to transmit vertical tensile stresses, but the study found that the method used to key the blocks together has important effects on how they would rock against each other, and potentially buckle, due to accelerations during an earthquake.

3.0 NEUTRON-IRRADIATION EFFECTS

Neutron damage in graphite occurs when fast neutrons displace carbon atoms from their equilibrium positions within the graphite crystal lattice [Burchell, 2008]. The resulting lattice strain can cause major structural and property changes in the graphite. Because the surface of the center reflector receives a large neutron dose, the design of the center reflector must take into account the effects of neutron damage in the graphite near the surface of the reflector. In this section, several methods for reducing neutron-induced stresses are examined.

3.1 Comsol Model

In order to analyze the neutron-induced stresses on the center reflector, a simplified model of the center reflector was developed in Comsol, which neglects the effects of crreep. While this simplified model also neglects much of the complicated geometry discussed in section 2.0 of the report such as coolant injection holes, several conclusions can be made regarding how to increase the lifetime of the center reflector.

3.1.1 Background

While Comsol is a powerful multi-physics finite element analysis (FEA) program used in a number of fields, the program lacks the capability to directly compute stresses due to neutron damage. Consequently, a thermal expansion study was performed, in which a temperature distribution was imposed on the model that yielded dimensional changes similar to dimensional changes resulting from neutron damage. The resulting thermal stresses at different years of operation were determined by solving the following governing equation:

$$S - S_0 = C:(\varepsilon - \varepsilon_0 - \varepsilon_{inelastic}) \quad (3.1)$$

where

$$\varepsilon_{inelastic} = \alpha(T - T_{ref}) \quad (3.2)$$

In equation 3.2, T_{ref} is a reference temperature and was chosen to be 540 K, α is the coefficient of thermal expansion for graphite, and the variable T is defined by equation 3.3:

$$T = 2.2990e2 * (year_t^2) - 6.1740e2 * (year_t) + 5.4624e2 \quad (3.3)$$

The variable $year_t$ is defined as the neutron fluence per year multiplied by the number of years. The neutron flux and fluence were determined using a simplified MCNP model of the center reflector. The MCNP code modeled the center reflector as a solid cylinder (with varying diameter) that lacked control rod holes, instrumentation holes, and channels for fluid flow.

Table 1 lists the material properties used in our model, which correspond to graphite grade IG-110. These values were taken from a paper discussing standards for graphite core components in a high temperature gas-cooled reactor (Eto et al., 2010). It should be noted, however, that the coefficient of thermal expansion listed in the paper does not correspond with the value we assumed for our model. This is due to the fact that we are simulating neutron damage by performing a thermal expansion study. Thus, this value was chosen (and equation 3.3 used to calculate the temperature) in order to give dimensional changes consistent with dimensional changes due to neutron damage. Lastly, the arbitrary reference temperature of 540 k was chosen to ensure that $T-T_{ref}$ could not be less than 0 kelvin at the lowest temperature, which corresponds to maximum shrinkage.

Table 1 Graphite Material Properties

Property	Value
Density (kg/m^3)	1740
Poisson's Ratio	0.14
Coefficient of Thermal Expansion (1/K)	3.6e-5
Young's Modulus, GPa	7.9
Peak Von Mises Stress (MPa)	35

3.1.2 Model Explanation

The stresses induced by neutron irradiation depend strongly on the geometry of the center reflector blocks. Our analysis was restricted to a cylindrical segment in the middle of the center reflector. As depicted below in figure 3.1, our initial model consists of a simple cylindrical disk of radius 35 cm and a height of 50 cm. A free boundary condition was applied in Comsol to all surfaces in the model. However, because Comsol is unable to compute a solution where all surfaces are free and since our simplified model does not include the keying structures used to keep the eight control-rod holes of each aligned symmetrically with the adjacent blocks, a small, cylindrical pin was placed in the center of the model and a fixed boundary condition was applied to the pin. While this allowed for a solution to be computed, the addition of the fixed pin resulted in an artificial buildup of stress in the center of the model. This small area of stress concentration was neglected when computing the peak stress in our analysis. Figures A.1 and A.2 in appendix A show respectively the fluence and the stress diagram of the block at one and two years of operation.

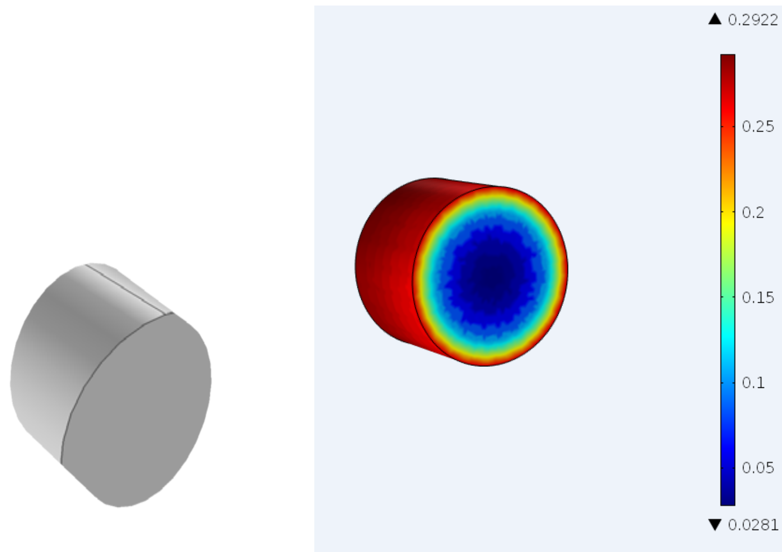

Fig. 3.1: Initial Comsol model (left), and the Comsol color plot (right) showing the fluence of the initial model at one year. The axis shows fluence in units of 10^{22} neutrons/cm^2.

As seen in the Von Mises stress diagrams in Fig. 3.2, the stress for a simple cylindrical block exceeds a Von Mises stress of 35 MPa after one year. While this calculation neglects creep effects that would reduce these stresses somewhat, they show that this simple cylindrical geometry is likely to be problematic.

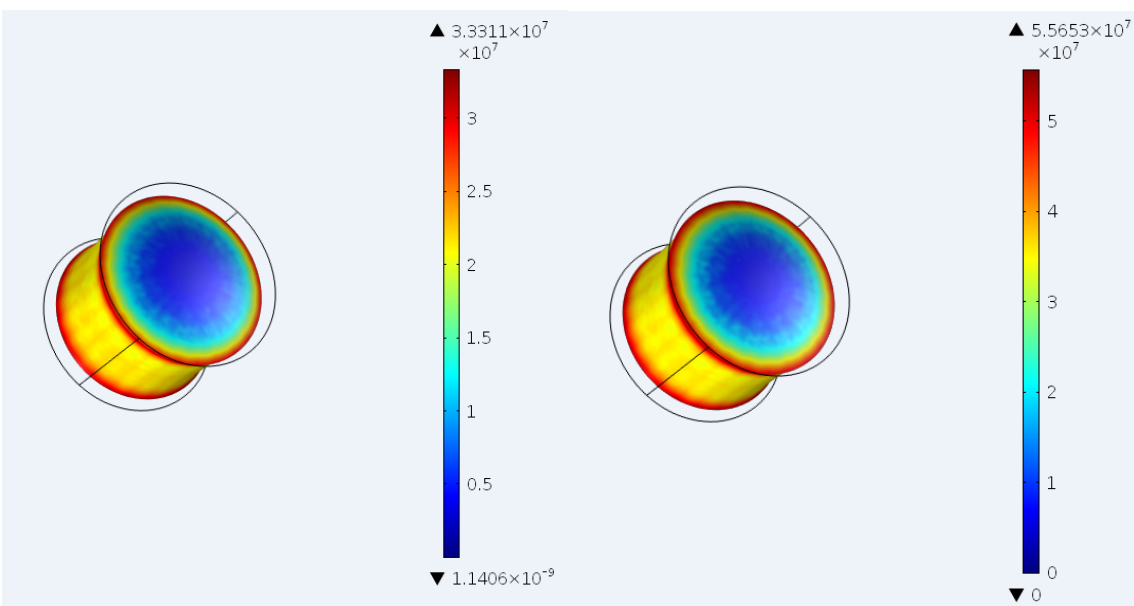

Fig. 3.2: Von Mises Stress diagram for the initial model at T = 1 year (left) and T= 2 years (right). The axis has units 10^7 Pa.

In order to make our analysis more realistic, we added eight holes that lie along the outer edge of the base of the block and continue through the whole block. The center of each hole is 27.6 cm far from the center of the cylinder. Since the radius of the hole is arbitrarily choses to be 6.2 cm, the center of each hole is 4.3 cm far from the edge of the block considering that the block has a 35 cm radius. These holes correspond to the control rod channels in the current center reflector design. The same fixed boundary condition is applied as for the simple block to calculate the peak stress for the new shape. Figure 3.3 shows the initial model with eight holes added.

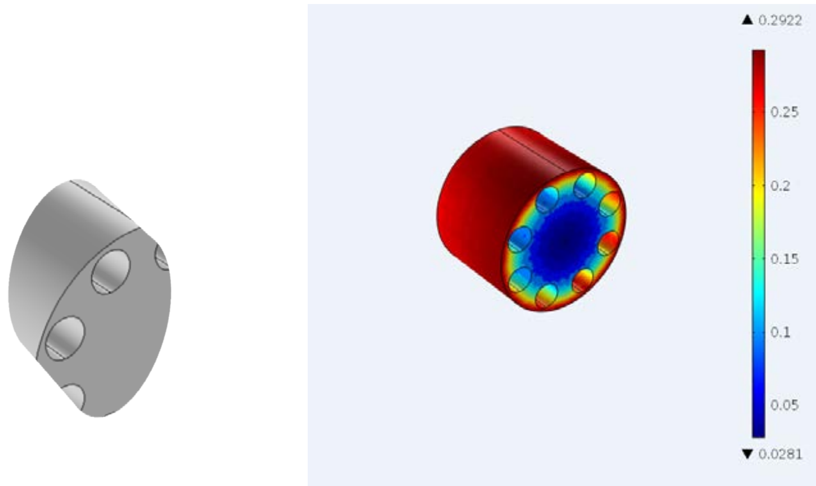

Fig. 3.3: Initial Comsol model with control rod channels added (left), and the Comsol color plot (right) showing the fluence of the initial model at one year. The axis shows fluence in units of 10^{22} neutrons/cm^{2}s

As seen in figure 3.4, the Von Mises stress for the cylinder with holes, the holes act to concentrate stresses and the peak stress exceeds the limit of 35 MPa before one year. Thus, we need to find ways to reduce the effects of neutron damage in order to increase the lifetime of the center reflector blocks. In the following sections of the report, we examine how changing the geometry of the block will affect the stresses. Our analysis includes studying the effects of cutting the piece horizontally, azimuthally and making a round shape edge around the hole so that the fast neutron fluence is always perpendicular to the surface of the control rod hole as it enters the block. More specifically, the cylindrical model with control-rod holes, depicted in figure 3.3 is initially partitioned into eight pieces (like a pie slice) and the stress distribution is computed for a single slice with different heights. Then, for a fixed height, the cylindrical model is cut into different pie slices with different angles. Finally, the thickness of the outer edge of the control rod hole is varied. It should be emphasized again that our model neglects the effects resulting from long-term creep deformation and consequently, is somewhat conservative.

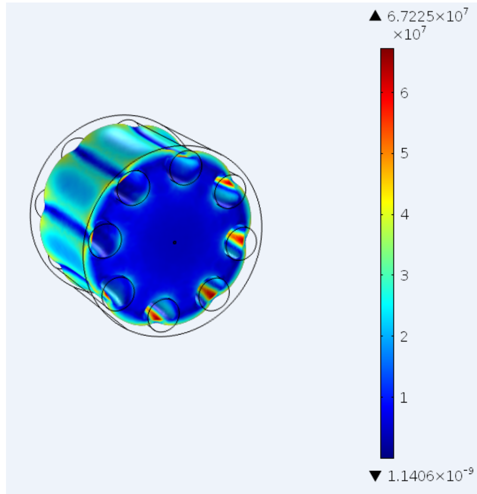

Fig. 3.4: Von Mises Stress diagram for the initial model with control rod holes at T = 1 year.

3.1.3 Previous Work

Previous studies modeling the effects of neutron damage on nuclear-grade graphite have been performed. One such study from the Institute of Nuclear Energy Technology at Tsinghua University in Tsinghua, China modeled the effects of neutron damage on rectangular graphite bricks over a period of thirty years using the finite element code ABAQUS [Marsden, Fok, and Li 2004]. The fast neutron dose was assumed to have a radial profile, with the neutron dose decreasing with increasing radius. The study reported axial and hoop stress histories—in contrast to our study, which reports the Von Mises Stress—at various times at power and at shutdown. Several conclusions were made from the study: namely, that hoop stresses were higher towards the end faces of the brick, that axial stresses were of a similar order to the hoop stresses, and that irradiation-induced creep reduces dimensional changes in the graphite brick due to neutron damage.

Also, the April 2014 edition of the Nuclear News had the interesting article "Torness Tackles Biggest-ever Outage" on the inspection procedure used in AGR (CO_2 gas-cooled, graphite moderated) reactors in the UK. Graphite inspection is a major part of the statutory outage. It is vital to supporting the safety case for continued operation of the reactor and it includes the use of a specialized camera to visually inspect the channels for degradation and any other issues regarding the condition of the graphite, the deployment of feeler gauges and other types of probes to measure features such as the ovality of the channels which is the level of tilt of the graphite bricks and the channel bore and finally the removal of small samples of the graphite for analysis which provides a greater understanding of the progress of graphite deterioration and other effects over its life cycle. Relying on the AGR's many practical experiences with managing graphite that has been irradiated by neutrons, we expect that the Comsol model for the MK1 center reflector blocks should predict the change in the "ovality" of the control rod channels due to neutron-induced dimensional changes, and this may provide a method to monitor for changes due to irradiation.

3.2 Stress vs. Height.

In this section, we examine how the height of the center refector blocks affects the peak Von Mises stress, by studying a slice of the block. Because the slice can bend, the predicted stresses are somewhat different from those for an actual full block (Fig. 2.2), but the analysis provides an understanding of the effects of height and allows us to identify an optimum height for the blocks. For this purpose, the model was sliced into eight equal pieces at a 45 degree angle, which was studied for varying heights of 10, 30, 50 and 70 centimeters.

3.2.1 Variation of height and exposure effects on Von Mises Stresses

Similar to the initial model, we defined a small cylindrical pin at the corner of the slice to serve as a fixed boundary condition, while all other surfaces were treated as free. While this allowed for a solution to be computed, the addition of the fixed pin resulted in an artificial buildup of stress in the corner of the model. Since the peak stress is expected to occur along the outer edge of slice near the control holes, the small area of stress concentration at the corner was neglected when computing the peak Von Mises stress.

The neutron fluence of a 50 cm high slice is depicted in Figure 3.5). Since the fluence diagram for the slice with the other heights is similar to the 50 cm high slice, the diagrams for others are not shown. Figure 3.6 shows the resulting Von Mises stress diagrams for the 50 cm high slice after two different periods of operation (the remaining cases are shown in Appendix A, Figs. A.1, A.2, and A.3). The first picture in each figure shows the peak stress at one year of operation and the second picture shows the year at which the slice fails.

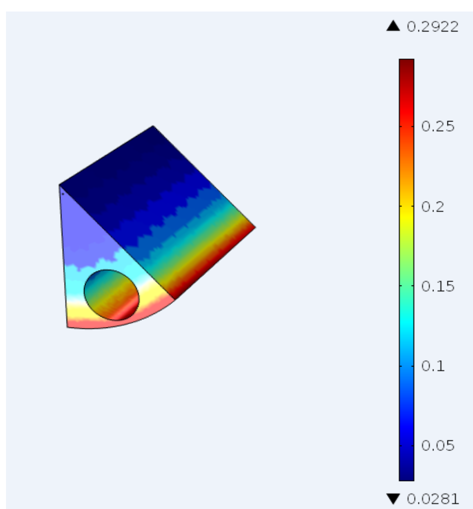

Fig. 3.5: The fluence of a 50 cm high slice at one year. The axis shows the fluence in units of 10^{22} neutrons/cm^2.

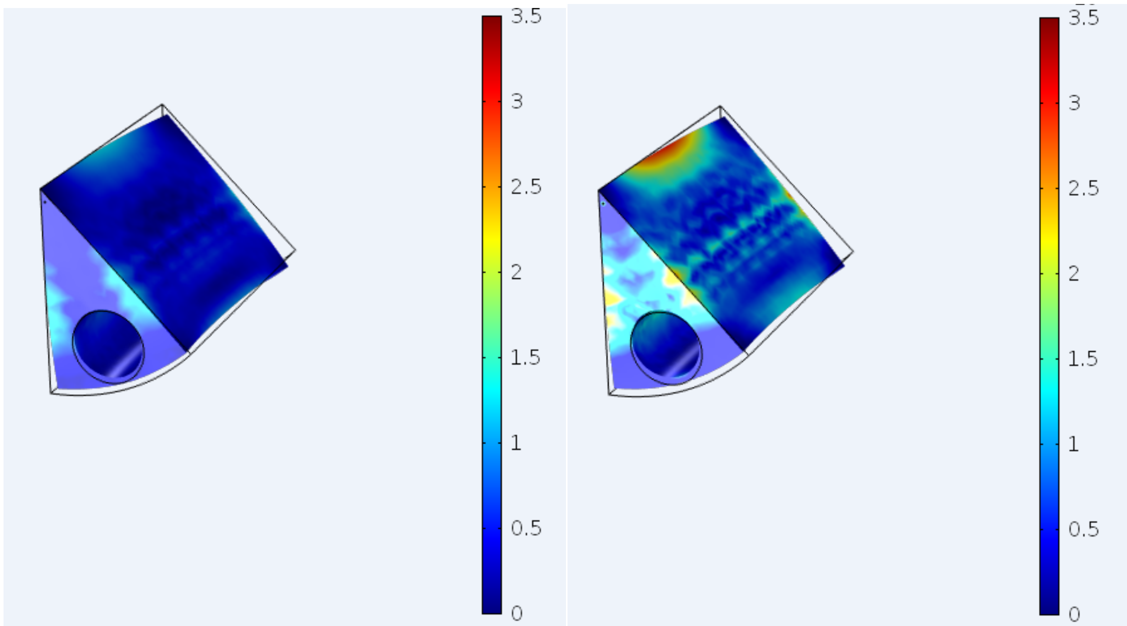

Fig. 3.6: Von Mises Stress diagrams for 50 cm high slice at T = 1 year (left) and T = 4 years (right). The axis has units of 10^7 Pa.

Examining the stress diagrams, none of the slices fail at one year of operation. The stress distribution at one year is almost uniform unlike at later times where the slices are close to failure. As time progresses, the stress distribution becomes increasingly non-uniform. In addition, the peak Von Mises stress increases as the height of the slice increases. The stress buildup for lower heights primarily occurs at the outer edge of the control rod channel, while, for slices with larger heights, the area with the largest Von Mises stress occurs at the corner edge of the slice. This is an artifact of the use of the slice geometry, since for an actual block each of the 8 lobes is connected at the center of the block (Figure 2.2). As a result, to avoid high edge stress buildup, the slices should be connected to each other at the corner of the slice (which is the center of cylinder). Since our model is greatly simplified and studied as an individual piece, our results will likely differ from results obtained by using the actual center reflector geometry and considering how the individual center reflector elements interface together.

3.2.2: Graphical Comparisons

Several graphs have been generated to demonstrate the correlation between peak Von Mises stress and the height of the block. Figure 3.7 shows the peak Von Mises surface stress as a function of height at years one and three. The peak Von Mises stress was found by computing the maximum surface stress. The surface that contains the cylindrical pin—which was created to play the role of a fixed boundary condition—was not included in the calculation to avoid the artificial stress buildup around the cylindrical pin. While computing the maximum volume stress would have been ideal, computing the max volume stress was not feasible with the pin stresses being considered.

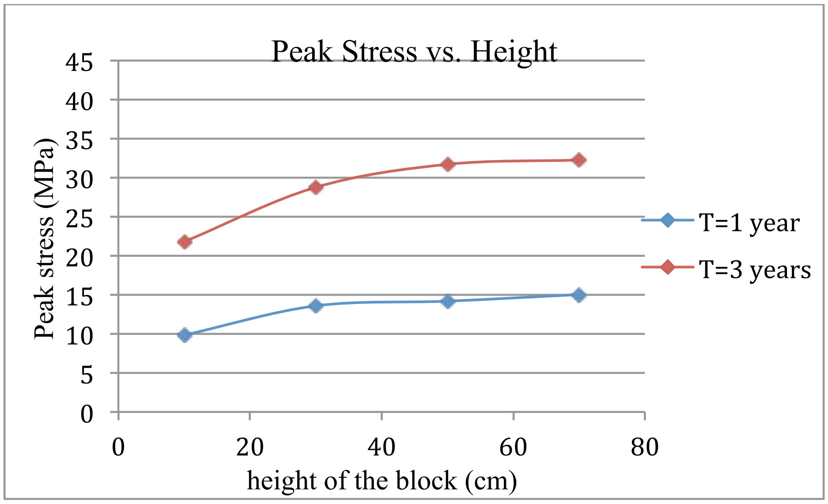

Fig. 3.7: Peak Von Mises stress as a function of height at one and three years of operation.

As seen in figure 3.7, the peak Von Mises stress approximately doubles at three years compared to the stress at one year for all the blocks. The 10 cm block has the lowest peak stress, while the other three block sizes have approximately the same stress at three years in the range of 25-35 MPa. As the figure suggests, the peak stress initially increases rapidly as the height increases and later approaches a maximum. The current baseline Mk1 block height of 25 cm (Figure 2.2) appears to provide a reasonable compromise between height and stress.

Figure 3.8 shows the lifetime (time to reach 35 MPa of each block as a function of its height. The lifetime for each block was determined by graphing the peak stress for each block size as a function of time and finding the intersection of the curve with a constant slope, horizontal line at 35 MPa.

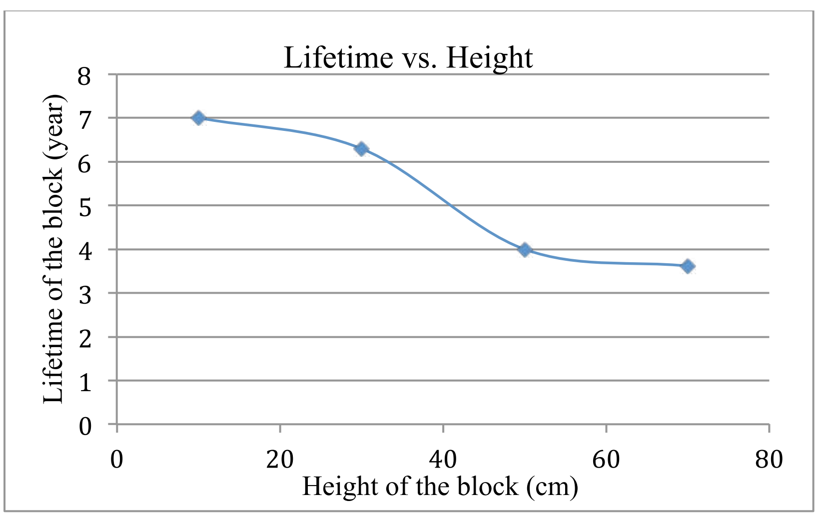

Fig. 3.8: Lifetime as a function of height.

Figure 3.8 suggests that thinner blocks would have longer lifetimes and that changing the block heights will vary the lifetime of the reflector blocks from 3.5-7 operating years. Figure 3.9 shows the peak stress as a function of time for four different heights of the block.

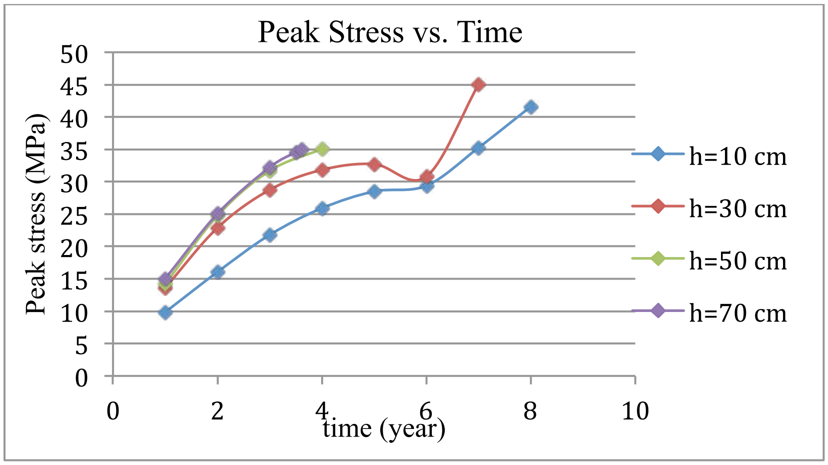

Fig. 3.9: Peak Von Mises stress as a function of time for blocks of four different heights.

Comparing the four graphs of peak stress as a function of time for the different heights, it is clear that the peak stress of the 10 cm block initially increases approximately linearly with time. The other three heights, in contrast, show more of an exponential increase. For the 30 cm tall block, we see a slight decrease in the stress just before it exceeds the limit of 35 MPa. This may be due to the thermal expansion of the graphite block, which in turn results in some stress distribution and reduction in the peak stress. As the height of the block decreases, the lifetime of the block (the amount of time it takes for the block to fail) increases, and as soon as the peak stress gets close to the stress limit, we see a sudden increase in the peak stress in a very short amount of time.

Now that we studied how changing height of the slice affects the peak stress endured by the block, we are interested to see if there is any correlation between changing the angle of the block with the peak stress experienced by it.

3.3 Stress vs. Angle

With an understanding of how changing height of the slice affects the peak stress endured by the block, this section will investigate if there is any correlation between angle of the studied block and experienced stresses. This would be useful in the design if we consider dividing the blocks along their outside radius to prevent stress concentrations. Specifically, this section investigates how the peak Von Mises stress varies depending on the angle of the slice. The height is fixed at 10 cm and several types of slices are examined with angles 30, 45, 60, and 90 degrees.

3.3.1: Variation of angle and exposure effects on Von Mises Stresses

The neutron fluence of a 45-degree slice is depicted in figure A.4 (the fluence diagrams for the other angles are essentially the same and are not shown), while the resulting Von Mises stress diagrams for all four slices are depicted in figures A.5, A.6, A.7, A.8, and A.9 at different years of operation. Note that the second picture in each figure shows the Von Mises stress diagram at a time after a peak Von Mises stress of 35 MPa has been reached (this time may differ for each angle).

As shown in the Von Mises stress diagrams, none of the slices experience a peak Von Mises stress exceeding 35 MPa at one year of operation. Additionally, the stress distribution seems fairly uniform for each slice. However, the 90-degree slice exhibits a buildup of stress in and around the control rod holes.

At seven or eight years of operation—depending on the slice—the stress distribution is far from uniform. In all slices, areas of peak stress occur in and around the control rod holes, with the 1.5-hole, 60-degree slice showing the greatest stress concentration along the outside of the control rod hole. The stress buildup along the outer edges of the control rod holes is possibly caused by the fact that the control rod holes are positioned very close to the outer edge of each slice. Positioning the control rod holes closer to the interior of each slice may reduce the large stresses experienced along the outer edges. This is examined in section 3.4 of the report.

3.3.2: Graphical Comparisons

To better assess the correlation between angle and peak Von Mises stress, it is helpful to graphically examine the relationship between the angle of the each slice and the peak Von Mises stress. Figure 3.10 shows the peak Von Mises stress as a function of angle at years one and five (the 1.5 hole, 60-degree slice is omitted since the peak stresses at the years plotted for the 1.5 hole slice are very close to the 60-degree, 1 hole slice). The peak Von Mises stress was determined by computing the maximum surface Von Mises stress in Comsol. The surface with the pin was, again, not included in the calculation, as the artificial buildup of stress around the pin would have led to unrealistic peak stress values for each slice.

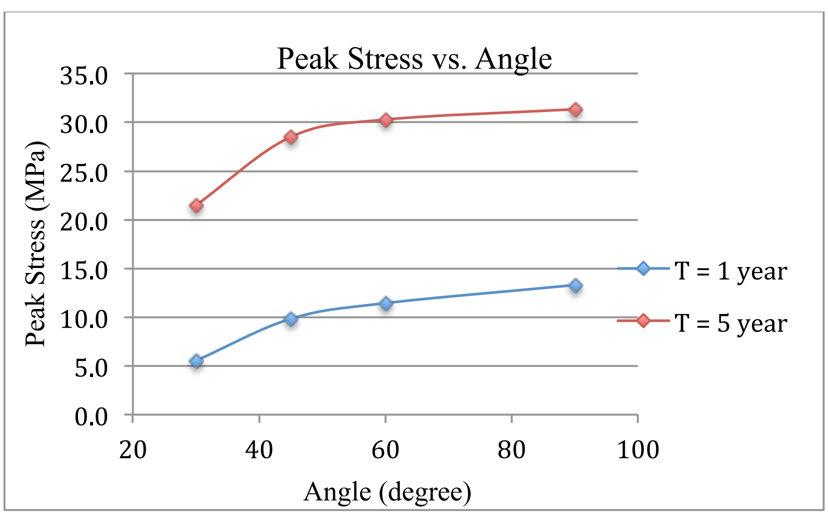

Fig. 3.10: Peak Von Mises stress as a function of angle at one and five years of operation. The 1.5 hole 60 degree slice is not included.

Figure 3.10 suggests that smaller angle slices experience a smaller peak Von Mises stress compared to larger angle slices. This is expected, since decreasing the angle of each slice should reduce azimuthal stresses. The figure also suggests that changing the angle of the cut has a greater effect on the peak Von Mises stress at smaller angles, as evidenced by the large difference in peak stress between a 30-degree slice and a 45-degree slice compared to a much smaller difference between a 60-degree and 90-degree slice.

As suggested by figure 3.11, all slices fail (exceed a peak Von Mises Stress of 35 MPa) within 6-8 years of operation. The figure provides a more precise comparison of the lifetimes of the different slices and depicts lifetime as a function of angle. The lifetime of each slice was determined by computing the peak Von Mises stress at each year, finding the year at which the peak Von Mises stress exceeded 35 MPa, and then interpolating between the year of failure and the previous year.

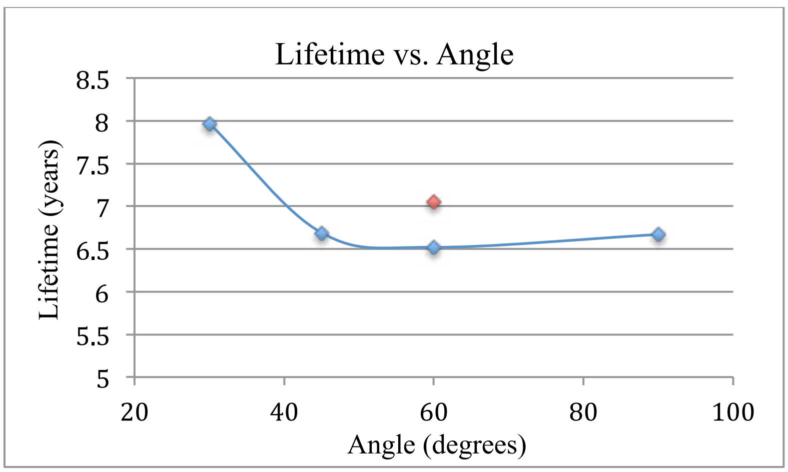

Fig. 3.11: Lifetime of slice as a function of angle. The red data point corresponds to the 60-degree slice with 1.5 control rod holes.

As expected, the 30-degree slice has the longest lifetime and lasts for approximately eight years. Larger angle slices generally have a smaller lifetime due to larger azimuthal stresses, with the 60-degree slice with the one control rod hole having the shortest lifetime. The 1.5 control rod hole, 60-degree slice and the 90-degree slice surprisingly have longer lifetimes than the 45-degree slice. This surprising result can perhaps be explained by examining figure 3.12, which shows peak stress vs. time for the different types of slices.

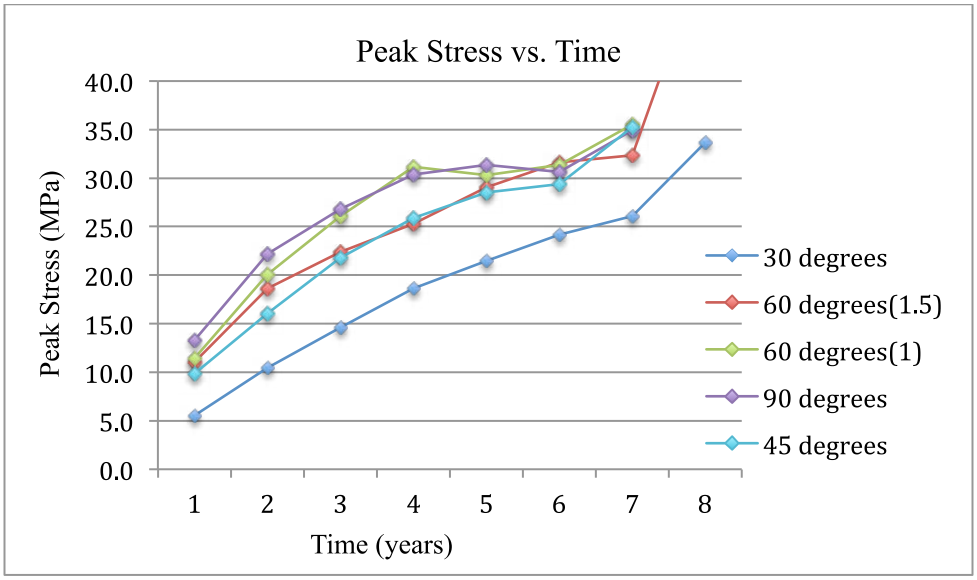

Fig. 3.12: Peak Von Mises stress as a function of time.

Examining the above figure, the 45-degree slice initially exhibits a lower peak stress than the 60-degree, 1.5-hole slice and the 90-degree slice. However, at later years the peak Von Mises stress of the 45-degree slice exceeds the peak Von Mises stress of the 1.5-hole, 60-degree slice (and the 90-degree slice near the failure point). At even later years, the peak stress of the 1.5 hole, 60-degree slice again exceeds the peak stress of the 45-degree slice. This behavior could possibly be caused by the buildup of an alleviating force around the control rod holes in the 90-degree and 60-degree (1.5 hole) slice. Since the control rod holes in the 90 and 60 (1.5) degree model cannot move freely like the single-holed 45-degree model, contraction forces may act further in the volume of the 90-degree and 60-degree model, which may, to a small extent, reduce stress near the outside of the model. This phenomenon would only occur after the contraction stress has migrated far enough into the model, which explains why the 60 and 90-degree model do not exhibit this behavior within the first four years. Another entirely plausible explanation is simply that our model is too simplistic to adequately model long-term neutron damage.

3.4 Stress vs. Control Rod Channel Wall Thickness

In this part, we analyze how changing the thickness of the graphite layer around the control rod channel affects the peak Von Mises stress experienced by the slice. For this purpose, three different wall thicknesses of 5, 6 and 7 cm are examined while the height of the slice is kept at fixed 10 cm and the angle is fixed at 45 degrees.

3.4.1: Variation of control rod thickness on Von Mises Stresses

Figure 3.9 shows the updated design of the block. While the initial block was exactly a slice of a circle, the new slice has a round wall around the control rod channel. With this new design, the fast neutron fluence is always perpendicular to the surface of the control rod channel. As before, the fixed boundary condition used for Comsol calculations is a cylindrical pin at the corner of the slice for which the buildup stress is high and is not included in the peak stress calculations of the slice. Figure 3.13 also shows the fast neutron fluence for the block. Since the fluence diagram for different wall thicknesses is similar, the diagrams are not shown for every single wall thickness. Figure 3.14 shows the peak Von Mises stress of the slice at one year of operation and at the time when the peak stress exceeds the limit of 35 MPa for a .   Appendix A contains figures for the other cases (Figs. A.

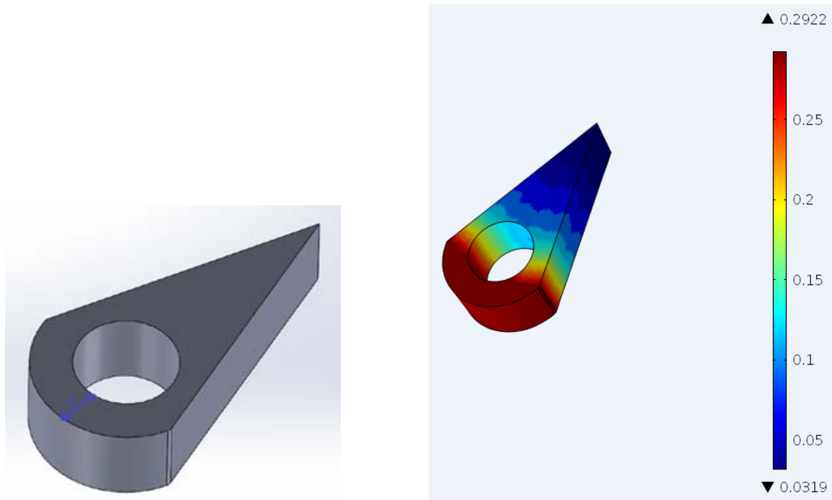

Fig. 3.13: Updated design of the slice with a round shape wall around the control rod channel (left) and fluence diagram (right).

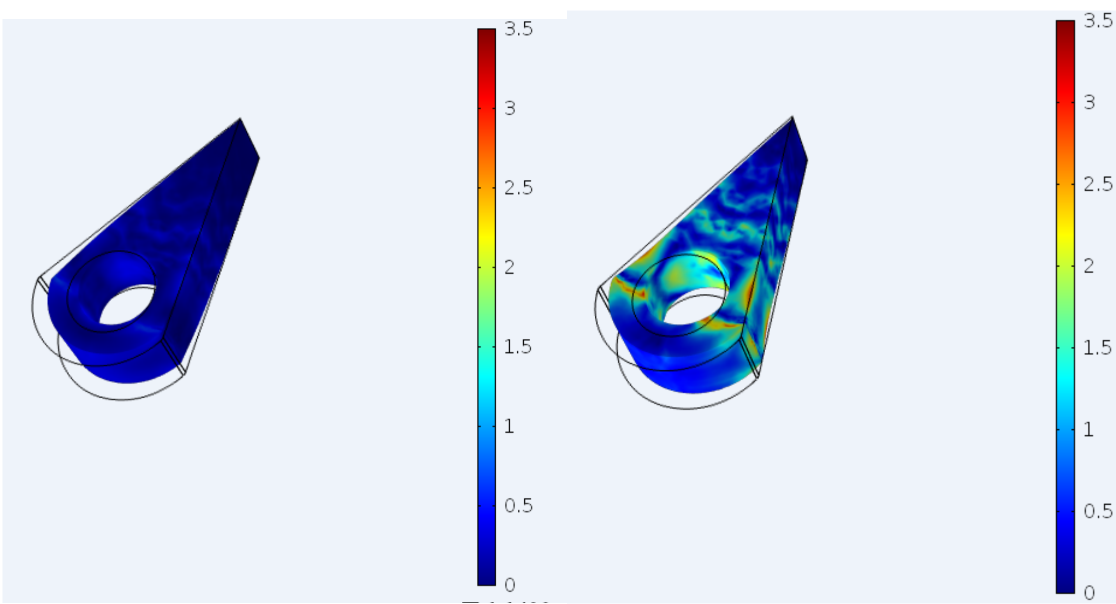

Fig. 3.14: Von Mises Stress diagrams for 10 cm high slice of round shape with d=5 cm at T = 1 year (left) and T = 8 years (right). The axis has units of 10^7 Pa.

The results of the stress diagrams show that making the graphite thickness around the control rod hole more uniform reduces the stress concentration significantly, and increases the service life of the reflector block.

3.4.2: Graphical Comparisons

This section will help us to look at and compare the behavior of slices with different wall thicknesses. Figure 3.15 shows peak Von Mises stress as a function of time for three different wall thicknesses.

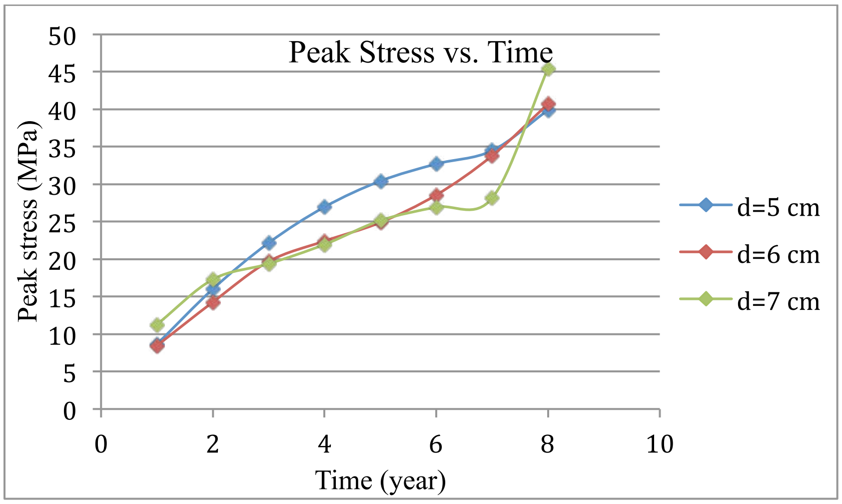

Fig. 3.15: Peak Von Mises stress as a function of time, where d equals wall thickness.

The above graph suggests that the block with the lowest wall thickness (5 cm) experiences higher Von Mises stress compared to the blocks with the other two thicknesses. It is interesting that the 6 cm wall thickness slice experiences the lowest stress in the beginning of the operation and the stress increases as time passes. However, the change in gradient of the stress is less compared to the 5 cm and 7 cm wall thickness slices. The slice with 7 cm wall thickness has a very similar behavior to the 6 cm one. However, it has a slightly higher peak stress at the beginning of the operation. Also, it has an unexpected rapid failure at the end where in one year the stress increases by more than 1.5 times its previous value (from 28 MPa to 45 MPa).

Again, while this analysis is preliminary and does not include the effects of creep, it indicates that the geometry of the center reflector blocks has a large effect on the peak stresses caused by fast neutron irradiation and on the likely block lifetime. It appears promising to develop geometries that can have service lives of 5 to 15 years, but more detailed analysis and design optimization will be required in the future to do this.

4.0 STATIC PUSHOVER TEST-ANALYTICAL MODEL

In considering the potential effect of seismic events on the Mk1 center reflector, we evaluated the static horizontal push-over acceleration needed to cause buckling of the reflector. Earthquakes also have vertical acceleration, but it is small relative to the horizontal acceleration. Therefore, we neglect vertical accelerations for the purposes of our calculations. Considering the force acting on the vertical direction, it will push the internal reflector upward and since it is fixed from the top, the force actually will help the system become more stable. To analyze the effect of horizontal acceleration, we segmented the center reflector into two sections—with the top potential hinge location in figure 4.1 separating the two sections—and looked at the force balance equations in x' and y' directions. Assuming a hinge at point A (the hinge location in the middle of Figure 4.1) and B (the hinge location at the bottom of Figure 4.1), we performed moment balances at the center of gravity for each piece (for a total of two moment balances).

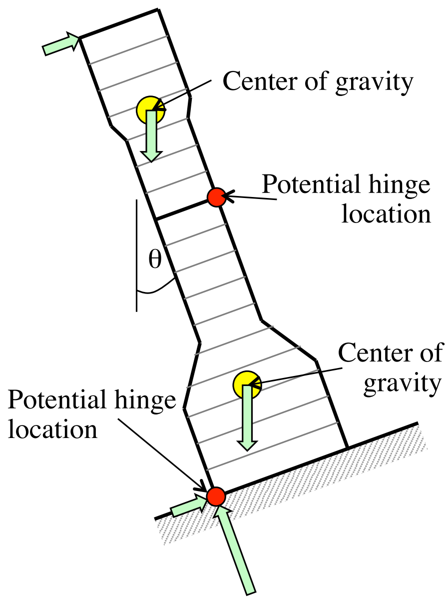

Figure 4.1: Basic diagram of static pushover test.

4.1 Explanation of model and analytical equations

4.1.1 Important Assumptions

Several assumptions were made in order to somewhat simplify the mathematical analysis of the static pushover test:

1. All forces are static; the moment of inertia has no effect on the analysis. As we perform the test, the reflector does not undergo any angular acceleration.
2. The point of "failure" is defined by a non-zero hinge angle. The model does not fail via slipping or material failure.
3. All motion occurs in the XY-plane (the plane of the page). There is no motion in the Z-direction (in or out of the page).

4.1.2 Free Body Diagrams

In order to analyze the forces applied during the static pushover test, we isolated one hinge-point/interface and separated the reflector into two pieces: the pieces above and below the hinge interface. We then determined all forces on each free-body, and used trigonometry to create expressions for all of the relevant moment-arms (distances from locations of applied force and the center of gravity). Both free-body diagrams along with supporting explanation can be found in Appendix B.

4.1.3 Analytical Equations

Using all of the forces and expressions for moment-arms, we then performed a moment balance on multiple points on the reflector. This resulted in six equations and six unknowns. We wrote a script in MATLAB (refer to Appendix B.4) to solve this system of equations four times to calculate the unknowns for each of the four trials of the static pushover test using the wooden model. This experiment, as well as a summary of the known variables and dimensions used to perform the analysis of each experimental trial, can be found in the section 5.1. The equations resulting from the force and moment balances at several points, as well as the MATLAB code used to calculate all of the unknowns, can be found in Appendix B.

4.1.4 Analytical Results

Trial	**Hinge Height (cm)**	**Angle of Failure (degrees)**	**Acceleration of Failure (% g)**
1	15.4	55.74	1.468g
2	12.38	49.43	1.168g
3	8.85	39.75	0.832g
4	5.73	27.59	0.523g

Table 4.1: Analytical results for four trials of wooden model static pushover experiment.

According to the analytical model, the higher the hinge in the experiment (the lower the hinge in the actual reactor), the larger the angle of pushover is required for failure by unhinging. The horizontal acceleration required for hinge-failure also follows this trend. This indicates that with the reflector oriented as it is in the Mk1, the block interfaces near the top of the reflector would be the weakest. A comparison with the experimental data can be found in section 5.1.4.

5.0 STATIC PUSHOVER TEST-EXPERIMENT

We performed two experiments to demonstrate the static pushover test; one with a scaled model of the center reflector, and one with a stack of tuna cans. This section contains information on experimental methods and results for both of these experiments.

5.1 Scaled Model

5.1.1 Experimental Preparation

The scaled model of the center reflector was machined out of a 5.0-cm diameter birch wood dowel. Due to the dimensions of this material, we scaled the full-sized center reflector so that the largest diameter of the central reflector corresponded to 5.0 cm (1:28 scaled model). It should also be noted that we used the older, “simple” model of the central reflector to both simplify analysis and fabrication. All of the dimensional scaling was performed in SolidWorks.

The wooden dowel was turned on a lathe in the Mechanical Engineering Student Machine Shop to machine the profile of the central reflector. A parting tool on the lathe was used to cut the model in four places to isolate four potential weak hinge points on the smallest diameter section of the reflector. (Of course, we finalized the fabrication process by decorating the reflector model with some Cal pride.) Figure 5.1 below shows a photograph the finished scaled model of the center reflector.

Figure 5.1: Scaled model of reflector used in experiment.

5.1.2 Important Dimensions and Measurements

We used SolidWorks "Mass Properties" evaluation tool in order to find the location of the center of gravities (CG) of each top and bottom pair corresponding to the four potential hinge situations (measured from the bottom). We required this information for predicting angles of failure according to our analytical model. The CG locations, as well as other important dimensions used are summarized in the experimental data table below.

Trial	Top Length (cm)	Bottom Length (cm)	Top Mass (g)	Bottom Mass (g)	CG Top (cm)	CG Bottom (cm)
1	5.2832	15.39748	23.1	81.6	17.4498	4.9276
2	8.29818	12.3825	31.5	73.2	16.2814	3.8608
3	11.82878	8.8519	41.2	63.5	14.732	2.8194
4	14.95552	5.72516	49.8	54.9	13.2842	2.1336

Table 5.1: Important dimensions and mass of wooden reflector model.

5.1.2 Experimental Methods

There were four trials in this static pushover experiment. Each trial corresponds to the isolation of one hinge at a time. In order to isolate one hinge at a time, we secured all of the other hinges closed with tape, and used tape on just one side of the joint of interest in order to create a hinge location and allow movement. Figure 5.2 shows the isolation of one hinge, allowing it to unhinge and rest of the hinge surfaces to remain in full contact.

Figure 5.2: Taping wooden model to isolate one hinge at a time.

We call this a static pushover test because we simulate the horizontal acceleration of the actual reflector by pushing it over while applying an opposing tangential force.

Because the actual reflector is lighter than the coolant in the Mk1 FHR, and floats upward, it rests against the upper core internals. In these experiments, which are dry, the reflector is turned upside down. Thus, from now on, use of the word "top" will refer to the actual bottom of the reflector, and use of the word "bottom" will refer to the actual top of the reflector. For each trial, we pushed the reflector over slowly at a constant speed, applying a tangential force to the top, until we saw the unrestricted hinge interface begin to unhinge. The angular displacement from the vertical was measured using a protractor. Figure 5.3 shows a picture of how the tangential force was applied to the wooden model.

Figure 5.3: Tangential force applied to top of wooden model during experiment.

5.1.3 Experimental Results

Trial	Hinge Height (cm)	Angle of Failure (degrees)	Acceleration of Failure (% g)
1	15.4	25 ± 0.5	0.466g
2	12.38	20 ± 0.5	0.364g
3	8.85	12 ± 0.5	0.213g
4	5.73	8 ± 0.5	0.141g

Table 5.2: Experimental results for four trials of wooden model static pushover experiment.

5.1.4 Comparison to Analytical Results

While the measured angles of failure and calculated accelerations of failure from the experiment are much less than those calculated from the analytical model, they still follow the same general trends discussed in section 4.1.4: the higher the hinge is off of the table, the higher the angle/horizontal acceleration required for hinging failure. We experimentally confirmed the conclusion drawn from the analytical solution: with the reflector in its actual orientation in the Mk1 reactor, the hinges closer to the top fail with less acceleration and angle of tilt than those near the bottom. Therefore, the hinges near the top of the reflector are the weakest in the case of a seismic event.

The discrepancy between the analytical and experimental angles of failure is mainly due to human experimental error. It is extremely difficult to apply a constant, horizontal force on the wooden model while tilting it. The analytical model assumes a completely static situation with a constant force at the point of hinge failure. If we were to repeat this experiment, we would design an experimental rig that assures a constant applied horizontal force, and perhaps even install a pressure transducer on the top of the wooden model. This would allow for us to monitor the applied force and adjust our experimental results according to any inconsistencies in the applied force across each experimental trial.

There was also some uncertainty in the measurement due to the lack of precision of the protractor (+/- 0.5 degrees), but this uncertainty was not enough to correct for the discrepancy between experimental and analytical results.

5.2 "Tuna Can" Static Pushover Test

In this experiment, a static pushover test is performed to observe where the column is stable and unstable in order to find out the angle in which the column transitions from being stable to unstable. This indicates where the graphite blocks of the center reflector can separate.

To calculate the static acceleration from the static test, the following formula was used:

$$a = g \times \tan\theta$$

where g = gravitational acceleration
θ =angle of the column with respect to the vertical

5.2.1 Experimental Design

In the reactor, the ends of the center reflector column are restrained from horizontal motions, with the net buoyancy force on the blocks being pushing upwards. Failure will then occur by "hinging" at joints between the graphite blocks. The main goal of this experiment is provide experimental results concerning this hinge problem and provide advice over the key design between blocks in order to carry the hinging loads during seismic acceleration.

5.2.2 Experimental Set up

The experiment is set-up so that the column of tuna cans is sitting on a fixed tuna can lid that is fixed on a movable platform. In this arrangement, the top of the center reflector of the nuclear reactor is represented by the bottom of our column. The gravitational forcing acting downward in from the tuna can column is similar to the buoyant force acting upward by the graphite block in the actual reactor. The bottom of the center reflector will be represented at the top of our stack of cans. The can lid will restrict side motion and act as a fixed position same as the top of the reactor where the top block is fixed by the equipment. On the side of the column, there is a support structure connected to a top plate. The top plate has a circular hole such that it will fit the can and restrict side movements of the can without impeding vertical axial movements. It represents the bottom of the actual center reflector which has a metal support base structure that restricts lateral horizontal movement and also holds the divider ring that separates reflector and fuel pebbles entering the bottom of the core, along with the 8 feed tubes used to inject the pebbles.

Fig. 5.4: Side view of the experimental setup.

The clearance of the diameter of the middle part of the can and the diameter of the hole of the restraining plate is 1.5% of the total diameter, which is in the same scale as the center reflector design since graphite would swell through irradiation. The experiment was designed to use two different scales. One setup had 10 cans, which corresponds to the real size of a 70 cm diameter and 307.8 cm height. The other setup involved 16 cans, corresponding to a 70 cm diameter with a height of 491 cm. The weight of each can was 442g. Each of set-up will undergoes two tests: one is the dynamic test to investigate on different hinge failure mode while the other one is a static test to investigate the angle which the blocks will become unstable.

5.2.3 Result With 10 Cans

The angle of failure was found to be 71.95° which corresponds to 3.07g. The reason for that is the top restraining plate providing a force that restrains the up and down movements along with its intended design to restrain side movements. Hence, the result is inaccurate. The hinge point for 10 cans is 123.12cm from the bottom of the center reflector column in reactor. Using the analytic model, the angle of failure was found to be 66.84 degree and the accelerating of hinge failure is 2.337g, it is actually quite close to the experimental result despite the error.

Fig. 5.5: Static experiment with 10 cans. Insipient stability of the stack is shown.

5.2.4 Result With 16 Cans

The distance from the bottom of the stack of cans where hinging occurred represents the real hinge distance from the top of the center reflector. The angle of the bottom of the can stack was 51.22° which correspond to a static acceleration of 1.24g while the angle of the top of the can stack was 40.35°. The angle of the opening at the hinge was found to be 10.87°. The hinge point for 16 cans is located 153.0cm from the bottom of the center reflector column in reactor. Using the analytic model, the angle of failure was found to be 50.06 degree and the accelerating of hinge failure is 1.194g, it is extremely close to the result of the actual experiment and it shows there is decreasing in angle with increasing total length.

Fig. 5.6: Static experiment with 16 cans. Insipient stability of the stack is shown.

6.0 PHYSICAL SEISMIC SIMULATION EXPERIMENT

In order to determine how the center reflector may behave under a seismic event, the same model discussed in section 5.2 was used in scaled experiments involving a shake table to determine the behavior of the center reflector during seismic events. Scaling considerations included the size of the central reflector and its height to diameter aspect ratio. This experiment utilized tuna cans and involved conducting a simple shaking test to examine the hinge failure mode.

6.1 Experimental Results for the Dynamic Shaking Test

Below is the displacement profile of the shaking test. The shaking test was conducted with a background with 2.5 cm equal-width black and white strips. Because the video is filming at 60 frames per second, the displacement profile was found by calculating the displacement frame by frame. Figures 6.1 and 6.2 present the calculated shaking history for the 10 can and 16 can shaking tests.

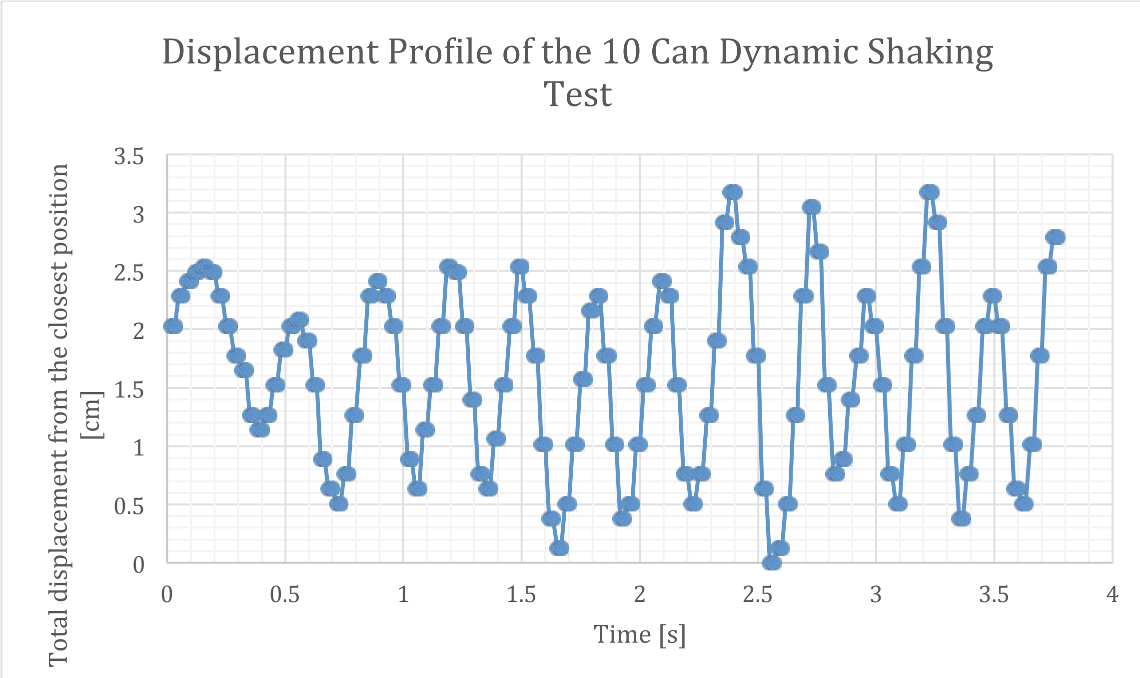

Fig. 6.1: Displacement Profile of the 10 Can Dynamic Shaking Test.

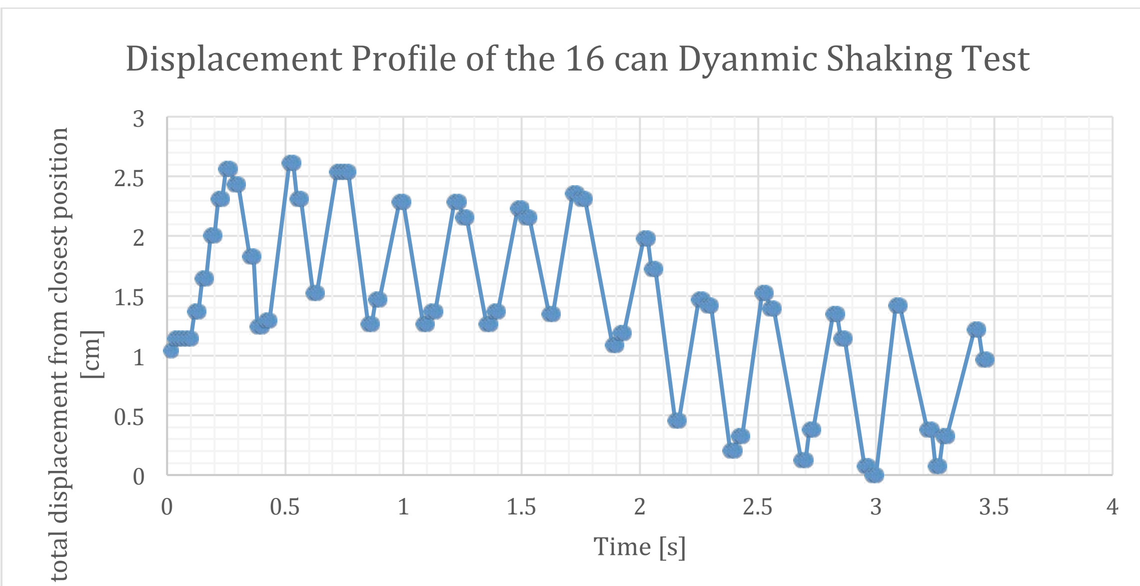

Fig. 6.2: Displacement Profile of the 16 Can Dynamic Shaking Test.

From the displacement profiles, we assumed the shaking test experiment underwent a simple harmonic motion represented by:

$$a = (2\pi f)^2 x$$

where a is the acceleration in m/s^2, f the frequency in Hz, and x the displacement from the center position in m.

6.3.1 Results from 10 can dynamic experiment

With an average frequency of 3.33 Hz and an average displacement of 10.3 mm at the onset of buckling, the peak acceleration was found to be 0.75g using the aforementioned equation of simple harmonic motion.

6.3: Shaking experiment with 10 cans. The moment of failure is shown.

The important result of this 10 cans seismic experiment is that the key failed to act as a hinge, in terms of properly interlocking the cans. This was indicated when the bottom slipped during the shake, as seen in Figure 6.3

6.3.2 Result from 16 can dynamic experiment

With an average frequency of 3.8 Hz and an average displacement of 5.87mm, the peak acceleration was found to be 0.45g by assuming simple harmonic motion.

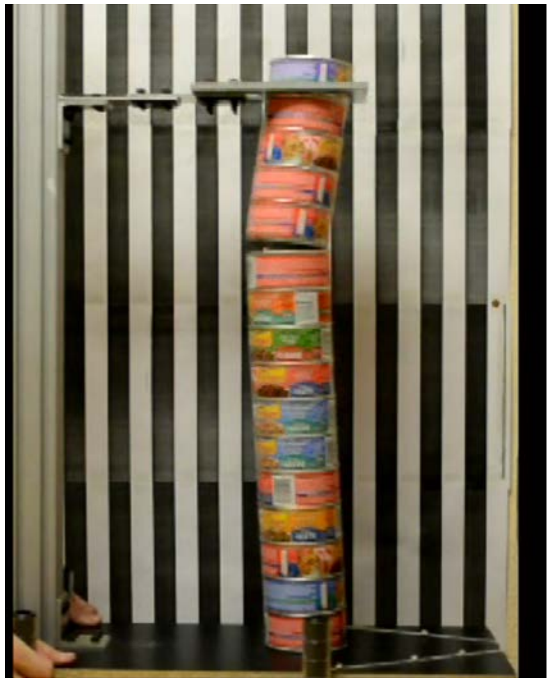

Fig. 6.4: Shaking experiment with 16 cans. The moment of failure is shown.

The keys worked as hinges as intended. A hinge formed around 18.7 cm from the top of the can stack, as shown in Figure 6.4, which indicates that this would occur 1.55 m from the bottom of center reflector. Before falling, the opening angle is 7.8°. For the center reflector, the size of this opening would be 9.5 cm. A 3 cm pebble can definitely slip in before the maximum hinge angle and pose a problem. The maximum angle which the opening would be less than 3cm correspond to an opening angle of 2.46°.

6.4 Conclusions of Dynamic Experiment

For the shaking experiment, we found it necessary to redesign the key (the circular double join design) to prevent slipping from occurring and make sure the key will works as hinge. Also, the opening gap may be large enough for 3 cm pebbles to pass through. This should be taken into consideration and we may need to have some mechanisms to block the pebbles from getting into the gap.

7.0 SUMMARY

While this study of neutron damage on the center reflector is based on a very simplified model without considering keyed structure, approximating neutron damage stress with a thermal stress and ignoring creep, it shows that the geometry of the center reflector blocks has a large effect on the peak Von Misses stress caused by fast neutron irradiation and on the lifetime. Several conclusions are made from this analysis. Lower heights of the block have lower peak stress. Smaller angles of the block have lower peak stress. Round shape wall around the control rod channel causes distribution of the observed peak stress at the outer edge for non-round shape wall around the wall increasing the lifetime of the block. Thus, it appears promising to develop the geometry of the block to get higher service lives. However, more detailed analysis and design optimization is required in the future to do this. The main conclusion from the analytical model and wooden model experiment was that the weakest hinges under the horizontal acceleration due to an earthquake are those nearest to the top of the reflector (in its true orientation in the reactor). Future work for the analysis should be to create a predictive model that includes key designs to interlock the reflector blocks. Ultimately, the predictive model should be able to predict multiple free interfaces that can fail by unhinging, rather than only the single free interface that our model currently describes. The wooden model experiment should be augmented and improved in accordance with the changes to the analytical model previously mentioned. This could include making a model that is somewhat closer in size to the actual reflector, is manufactured out of a different material, has interlocking keys between blocks, has the "flower-like" cross sectional geometry of the current reflector design, has control rod holes, and is composed of more total blocks. In addition to improving the model used in the experiment, the experimental procedure should be improved. The next experiment with the improved model would be to suspend the reflector in the proper orientation (from the top), in a tank of fluid to simulate FLiBe. The experimental setup should be placed on a shake-table in order to simulate varying amplitudes and frequencies of earthquakes. Ideally, the experimental setup should be outfitted with various sensors (displacement, stresses, accelerometer) to gain useful data about the structural performance of the reflector under earthquake-induced stresses.

From static tuna can experiment, it have high degree of consistence with the analytical model and it reveal that the block opening may become an issue that in the real reactor, a 3cm pebbles may get through the gap and create problem. In the shaking experiment, it reveal different failure model of the tuna can. The hinge either failed to work and the tuna can just slipped or the tuna can side work as hinge and prevent slipping. Future study need to be done for the joint (key) design that will act as hinge and bear the load. Also, other study needs to be conducted regarding the issue of black opening because the shaking experiment that we conducted did not contain pebbles around the car act as damping.

8.0 REFERENCES

C. Andreades, A. T. Cisneros, J.K. Choi, A.Y.K. Chong, D. L. Krumwiede, L.R. Huddar, K. Huff, M. R. Laufer, M.O. Munk, R.O. Scarlat, J. Seifried, N. Zweibaum, E. Greenspan, and P. F. Peterson, 2014, "Technical Description of the 'Mark 1' Pebble-Bed Fluoride-Salt-Cooled High-Temperature Reactor (PB-FHR) Power Plant," Department of Nuclear Engineering, U.C. Berkeley, Report UCBTH-14-002.

Burchell, Tim. "Neutron Irradiation Damage in Graphite and Its Effects on Properties." *Oak Ridge National Laboratory*. Oak Ridge National Laboratory, 2008. Web. 20 Apr. 2014.

S.L. Fok, H. Li, and B.J. Marsden, 2004, "Relationship between nuclear graphite moderator brick bore profile measurement and irradiation-induced dimensional change," Department of Nuclear Engineering, Tsinghua University.

Kovan, Dick. "Torness Tackles Biggest-ever Outage." *Nuclear News* April (2014): 43-48. *American Nuclear Society*. Web. 15 May 2014.

M. Eto, E. Kunimoto, T. Maruyama, T. Oku, K. Sawa, T. Shibata, and S. Shiozawa, "Draft of Standard for Graphite Core Components in High Temperature Gas-cooled Reactor," JAEA-Research 2009-042.

APPENDIX A: Von Mises Stress Diagrams

A.1 Stress vs. Height Diagrams

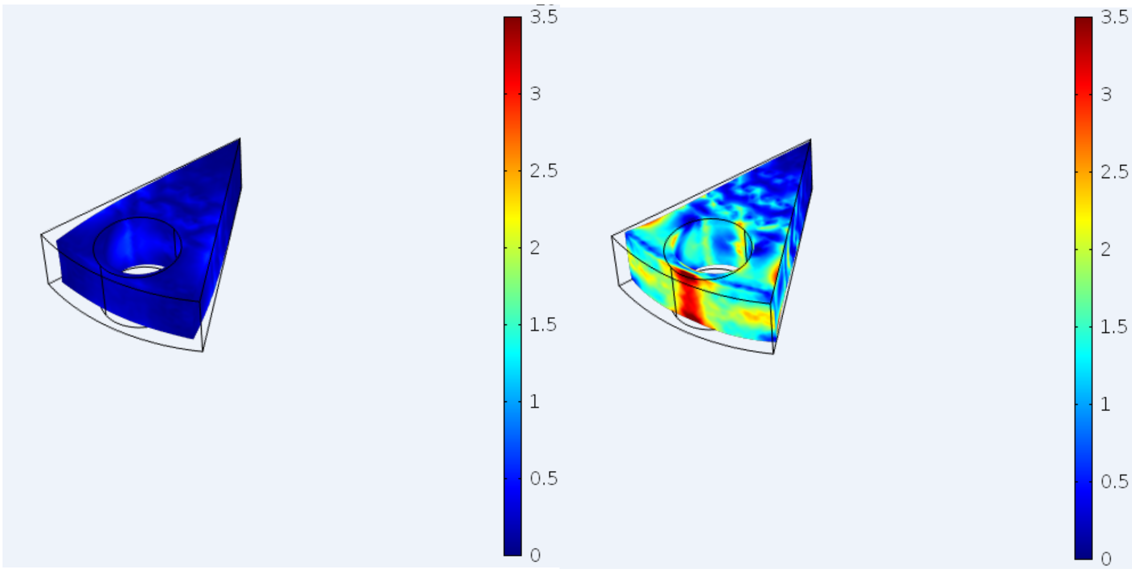

Fig. A.1: Von Mises Stress diagrams for 10 cm high slice at T = 1 year (left) and T= 8 years (right). The axis has units of 10^7 Pa.

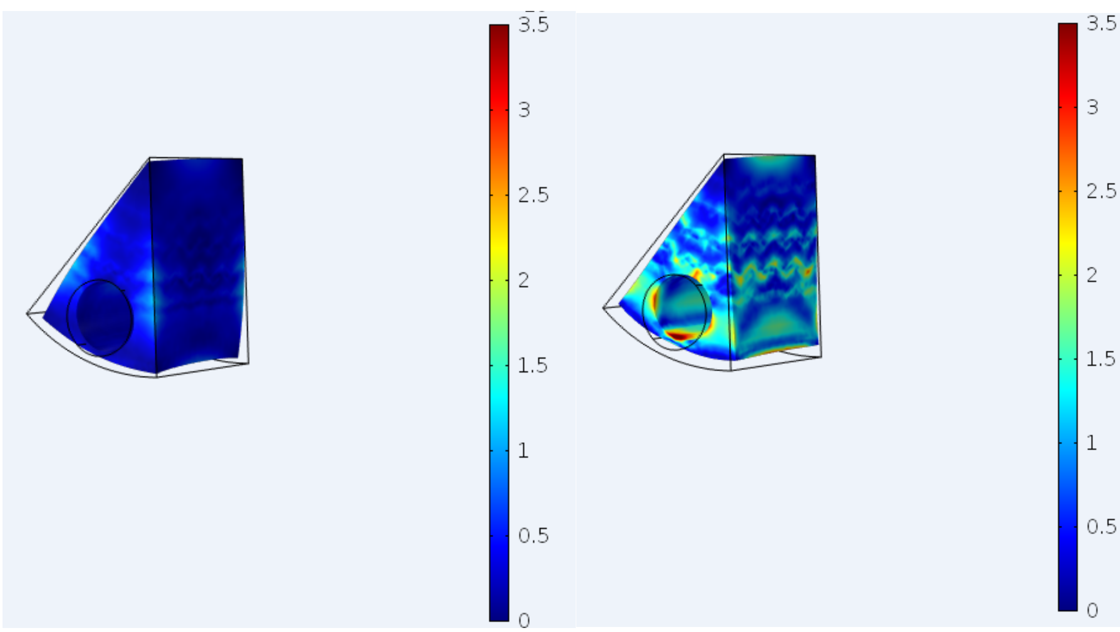

Fig. A.2: Von Mises Stress diagrams for 30 cm high slice at T = 1 year (left) and T = 7 years (right). The axis has units of 10^7 Pa.

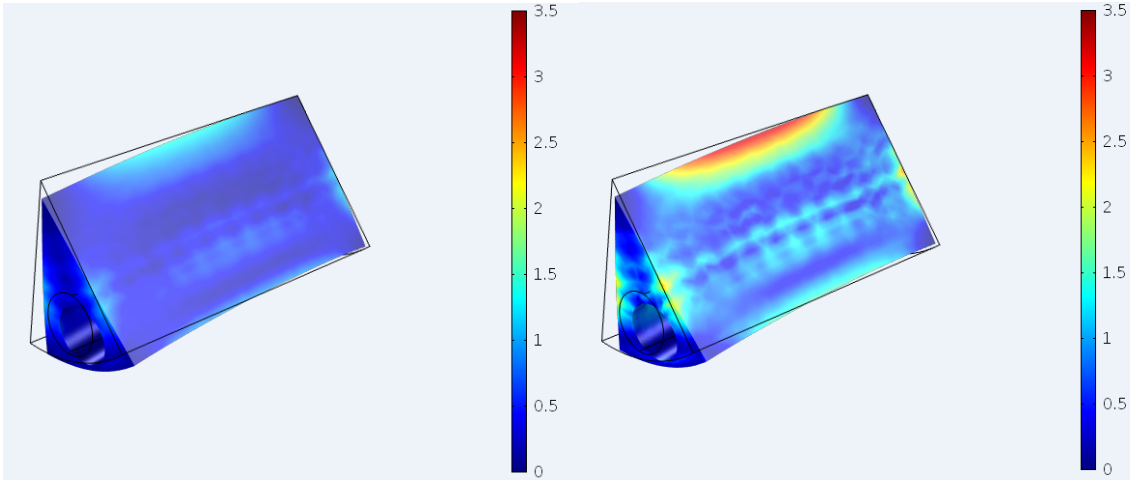

Fig. A.3: Von Mises Stress diagrams for 70 cm high slice at T = 1 year (left) and T= 3.616 years (right). The axis has units of 10^7 Pa.

A.2 Stress vs. Angle Diagrams

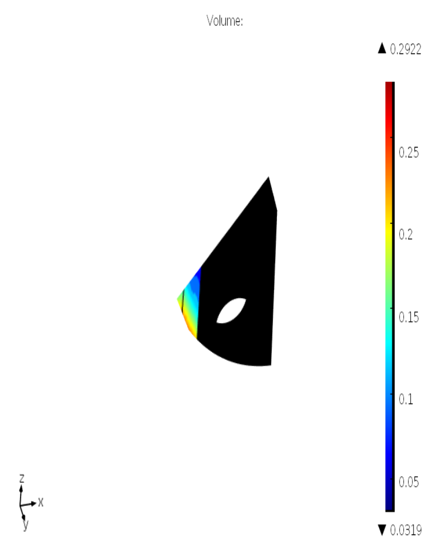

Fig. A.4: Fluence of a 45-degree slice at one year. The axis shows fluence in units of 10^{22} neutrons/cm^2.

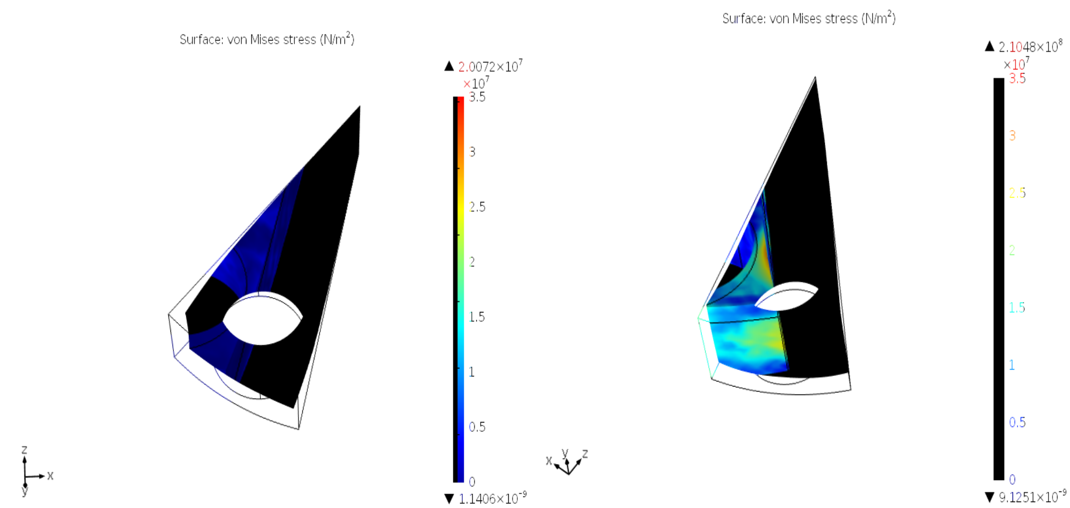

Fig. A.5: Von Mises Stress diagrams for 30-degree slice at T = 1 year (left) and T = 8 years (right). The axis has units of 10^7 Pa.

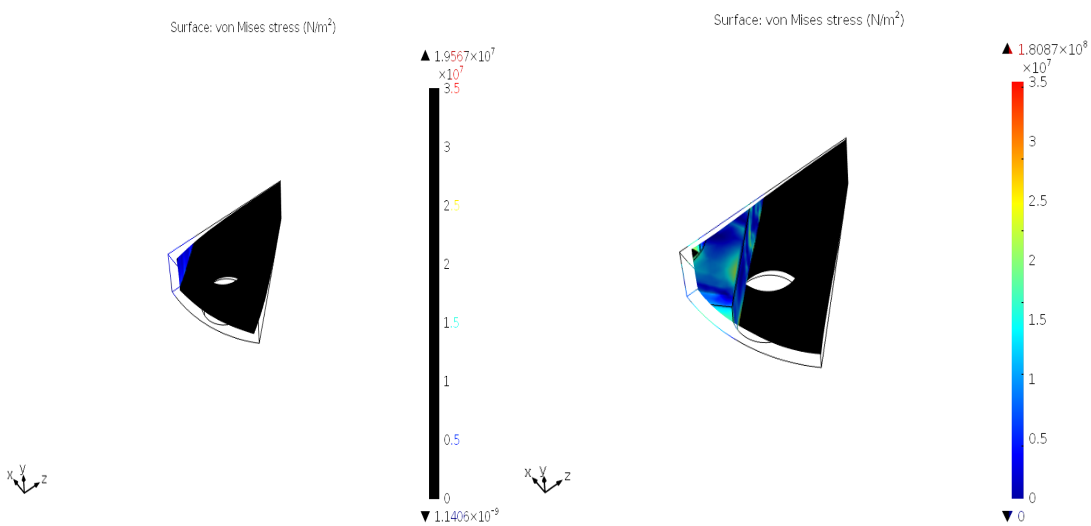

Fig. A.6: Von Mises stress diagrams for 45-degree slice at T = 1 (left) and T = 7 years (right). The axis has units of 10^7 Pa.

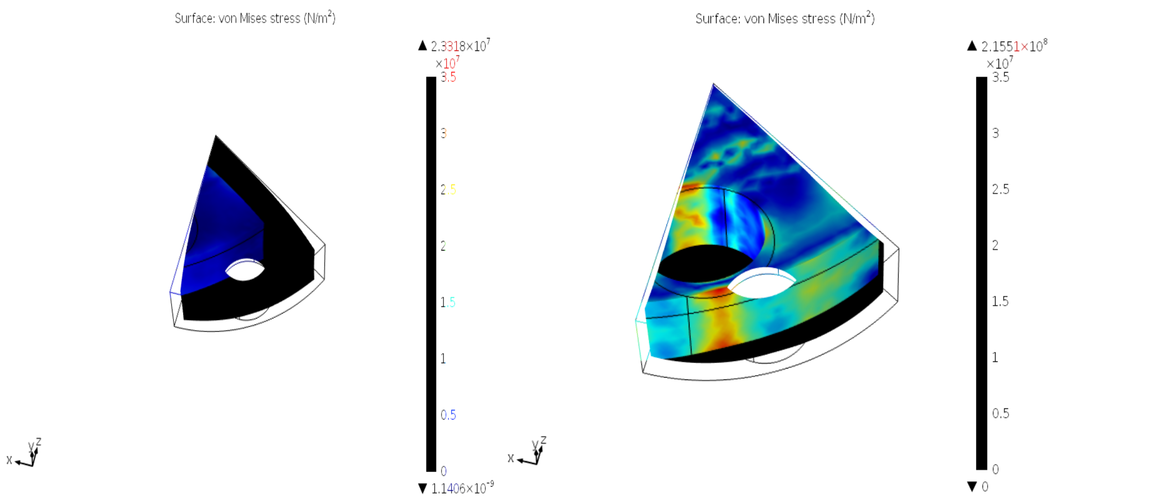

Fig. A.7: Von Mises stress diagrams for 60-degree slice at T = 1 (left) and T = 7 years (right). The axis has units of 10^7 Pa.

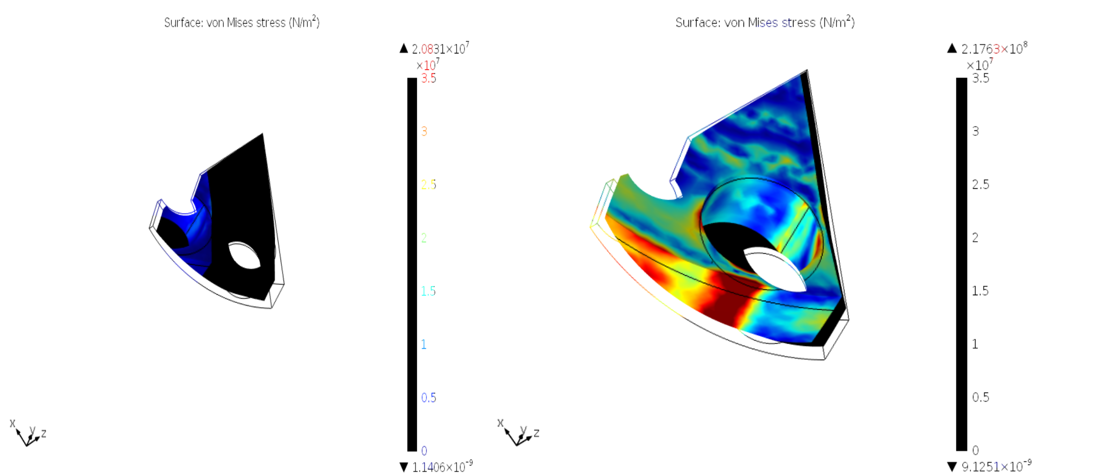

Fig. A.8: Von Mises stress diagrams for 60-degree slice with 1.5 control rod holes at T = 1 (left) and T = 8 years (right). The axis has units of 10^7 Pa.

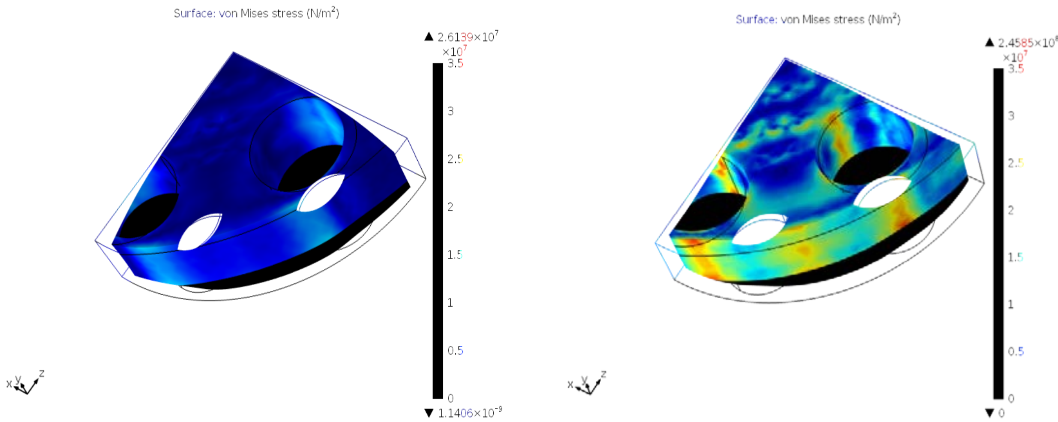

Fig. A.9: Von Mises stress diagrams for 90-degree slice at T = 1 (left) and T = 7 years (right). The axis has units of 10^7 Pa.

A.4 Rounded wall design fluence and stress diagrams.

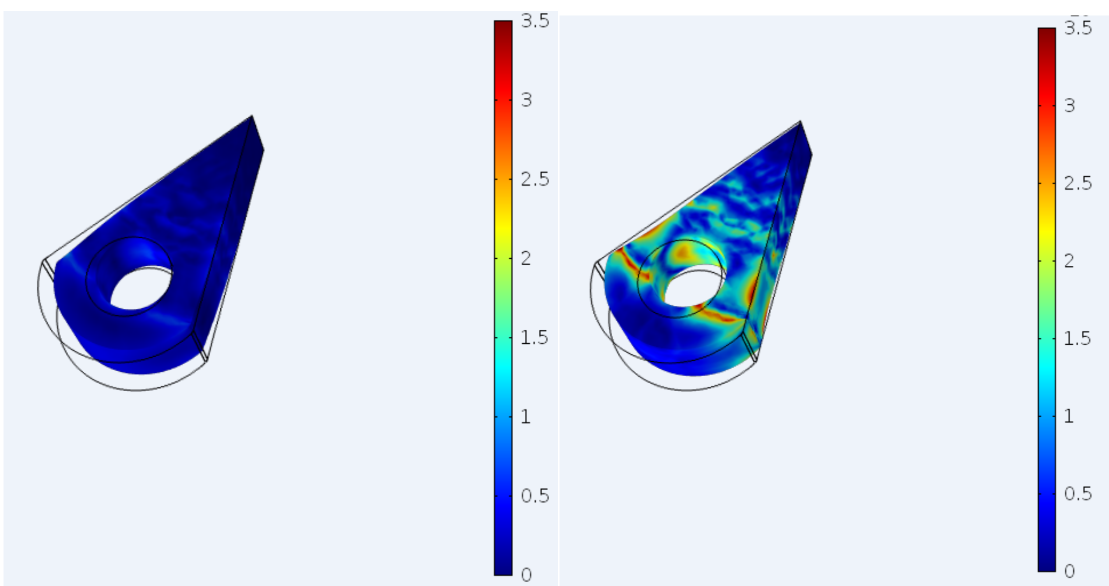

Fig. A.10: Von Mises Stress diagrams for 10 cm high slice of round shape with d=6 cm at T = 1 year (left) and T = 8 years (right). The axis has units of 10^7 Pa.

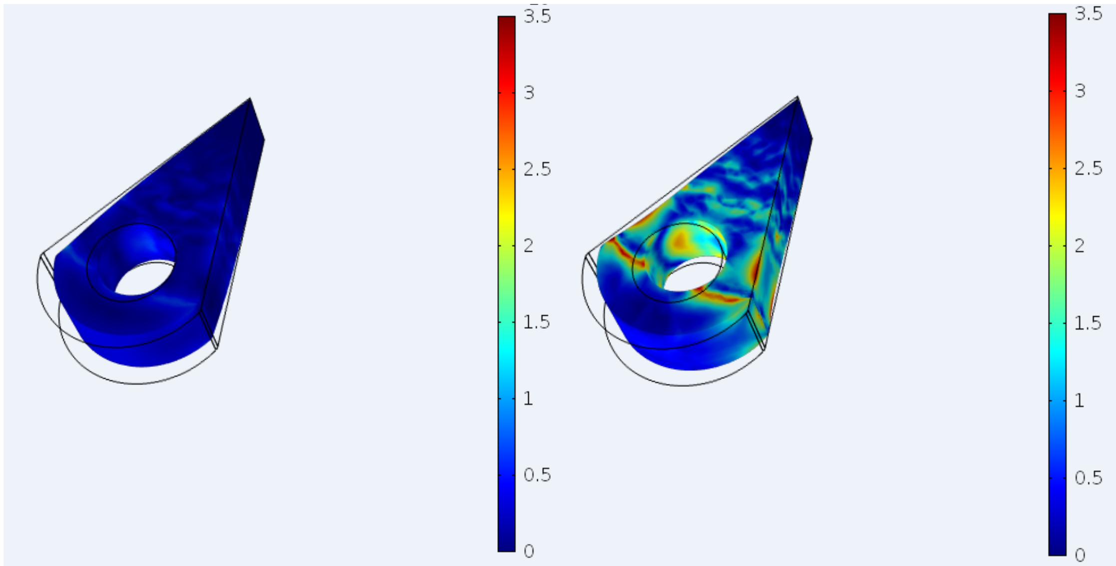

Fig. A.11: Von Mises Stress diagrams for 10 cm high slice of round shape with d=7 cm at T = 1 year (left) and T = 8 years (right). The axis has units of 10^7 Pa.

APPENDIX B: ANALYTICAL MODEL

B.1 Top Piece Free Body Diagram

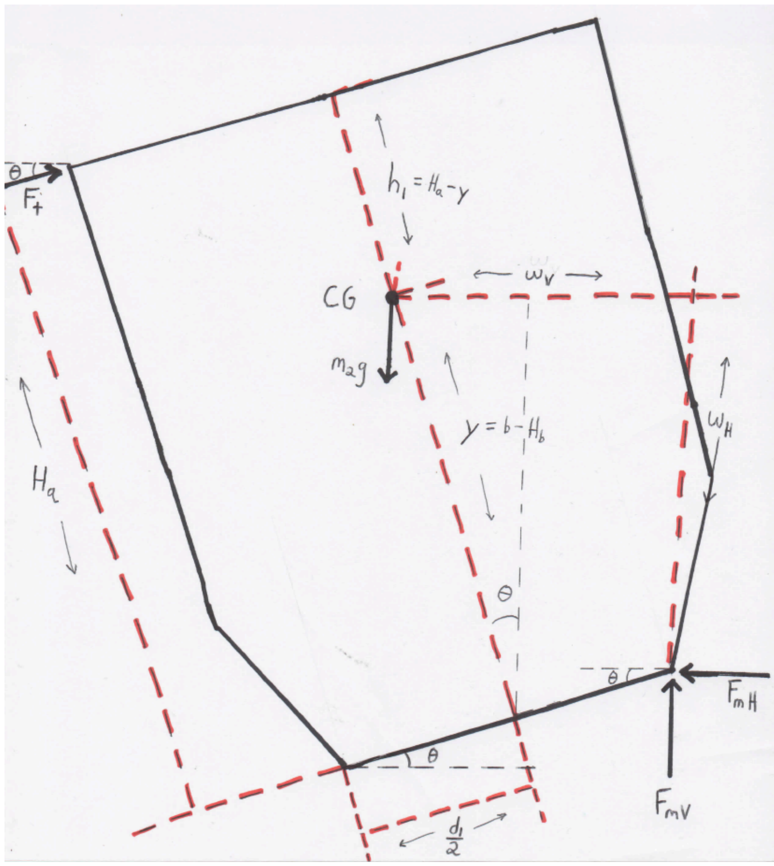

Figure B.1: Free Body Diagram of Top Piece in Static Pushover Experiment

There are several important features in Figure B.1:

- The force due to gravity is applied at the center of gravity.
- F_t represents the horizontal applied force during the experiment.
- F_{mV} and F_{mH} are the vertical and horizontal contact forces between the top and bottom pieces.
- Some of the important dimensions used in the analytical solution were determined using the geometry of the piece, and are summarized below:

$$h_1 = H_a - y$$

$$w_H = y\cos\theta - \frac{d_1}{2}\sin\theta$$

$$w_V = y\sin\theta + \frac{d_1}{2}\cos\theta$$

B.2 Bottom-piece free body diagram.

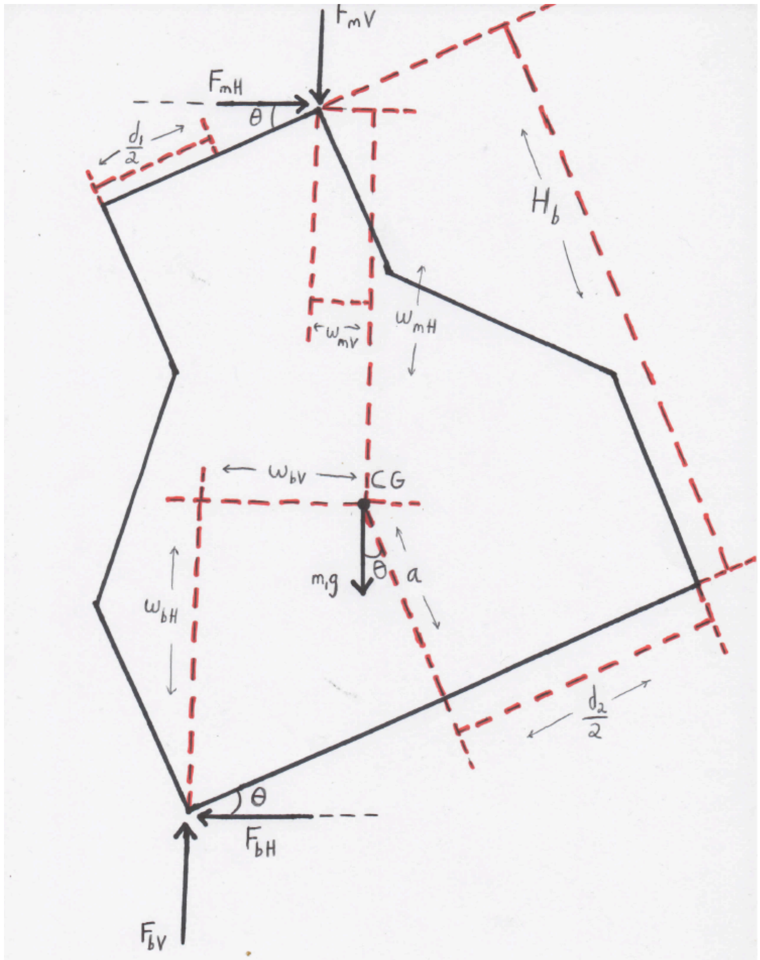

Figure B.2: Free Body Diagram of Bottom Piece in Static Pushover Experiment

There are several important features in Figure B.2:

- The force due to gravity is applied at the center of gravity.
- F_{mV} and F_{mH} are the vertical and horizontal contact forces between the top and bottom pieces.
- F_{bV} and F_{bH} are the vertical and horizontal contact forces between bottom piece and the table.
- Some of the important dimensions used in the analytical solution were determined using the geometry of the piece, and are summarized below:

$$w_{bH} = a\cos\theta + (\frac{d_2}{2} - a\sin\theta)\sin\theta$$
$$w_{bV} = (\frac{d_2}{2} - a\sin\theta)\cos\theta$$
$$w_{mH} = (H_b - a)\cos\theta + \frac{d_1}{2}\sin\theta$$
$$w_{mV} = (H_b - a)\sin\theta - \frac{d_1}{2}\cos\theta$$

B.3 Analytical Equations from force and moment balance

Below is a summary of the six equations obtained from performing force and moment balances on both the top and bottom pieces. Definitions of all the known dimensions (labeled in the two free body diagrams above) are also included.

(1) $$F_t\cos\theta = F_{mH}$$

(2) $$F_t\sin\theta + F_{mV} = m_2 g$$

(3) $$F_t(H_a - y) + F_{mH}(y\cos\theta - \frac{d_1}{2}\sin\theta) = F_{mV}(y\sin\theta + \frac{d_1}{2}\cos\theta)$$

(4) $$F_{mH} = F_{bH}$$

(5) $$F_{bV} = F_{mV} + m_1 g$$

(6) $$F_{mH}[(H_b - a)\cos\theta + \frac{d_1}{2}\sin\theta] + F_{bV}[(\frac{d_2}{2} - a\sin\theta)\cos\theta] + F_{bH}[a\cos\theta + (\frac{d_2}{2} - a\sin\theta)\sin\theta]$$
$$= F_{mV}[(H_b - a)\sin\theta - \frac{d_1}{2}\cos\theta]$$

Unknowns (6):
θ, F_{mH}, F_t, F_{mV}, F_{bH}, F_{bV}

Known Variables:
m_1 - mass of bottom part
m_2 - mass of top part
H_a - height of top part
H_b - height of bottom part
a - center of mass for bottom part (measured from bottom of entire stack)
b - center of mass for top part (measured from bottom of entire stack)
y = b - H_b - distance from bottom of top part to its center of mass
d_1 - diameter of thin section
d_2 = diameter of thickest part of bottom piece

B.4: Use of MATLAB to Solve System of Equations

We wrote a script in MATLAB to solve the system of equations and provide analytical predictions of angle of hinge-failure and corresponding horizontal accelerations of failures (for each of the four trials). It first defined all of the known variables for each trial, and then uses the built in "solve" function to solve the system of equations. After all six unknowns are solved for, it performs some simple math to calculate the angles of failure (from the vertical), and the corresponding horizontal accelerations. Below is the MATLAB code:

```
% mass of BOTTOM part for each trial [kg]
m1 = [0.0816, 0.0732, 0.0635, 0.0549];
% mass of TOP part for each trial [kg]
m2 = [0.0231, 0.0315, 0.0412, 0.0498];

% height of TOP part for each trial [m]
H_a = (2.54/100).*[2.08, 3.267, 4.657, 5.888];
% height of BOTTOM part for each trial [m]
H_b = (2.54/100).*[6.062, 4.875, 3.485, 2.254];

% acceleration due to gravity [m/s^2]
g = 9.81;

% center of mass for BOTTOM part (measured from bottom of stack) [m]
a = (2.54/100).*[1.94, 1.52, 1.11, 0.84];
% center of mass for TOP part (measured from bottom of stack) [m]
b = (2.54/100).*[6.87, 6.41, 5.8, 5.23];

% defining y
y = b - H_b;

% diameter of thin section [m]
d1 = (2.54/100)*0.986;
% diameter of thickest part of bottom piece [m]
d2 = (2.54/100)*2;

% define 6 unknowns to solve
syms F_t theta F_mH F_mV F_bH F_bV

% solve system of equations for each trial
S1 = solve(F_t.*cos(theta) - F_mH, F_t.*sin(theta) + F_mV -m2(1).*g,...
F_t.*(H_a(1) - y(1)) + F_mH.*(y(1).*cos(theta) - 0.5.*d1.*sin(theta)...
) - F_mV.*(y(1).*sin(theta) + 0.5.*d1.*cos(theta)), F_mH - F_bH,...
F_bV - F_mV - m1(1).*g, F_mH.*((H_b(1) - a(1)).*cos(theta) + 0.5.*...
d1.*sin(theta)) + F_bV.*((0.5.*d2 - a(1).*sin(theta)).*cos(theta)) +...
F_bH.*(a(1).*cos(theta) + (0.5.*d2 - a(1).*sin(theta)).*sin(theta))...
- F_mV.*((H_b(1) - a(1)).*sin(theta) - 0.5.*d1.*cos(theta)));
S2 = solve(F_t.*cos(theta) - F_mH, F_t.*sin(theta) + F_mV -m2(2).*g,...
F_t.*(H_a(2) - y(2)) + F_mH.*(y(2).*cos(theta) - 0.5.*d1.*sin(theta)...
) - F_mV.*(y(2).*sin(theta) + 0.5.*d1.*cos(theta)), F_mH - F_bH,...
F_bV - F_mV - m1(2).*g, F_mH.*((H_b(2) - a(2)).*cos(theta) + 0.5.*...
d1.*sin(theta)) + F_bV.*((0.5.*d2 - a(2).*sin(theta)).*cos(theta)) +...
F_bH.*(a(2).*cos(theta) + (0.5.*d2 - a(2).*sin(theta)).*sin(theta))...
- F_mV.*((H_b(2) - a(2)).*sin(theta) - 0.5.*d1.*cos(theta)));
S3 = solve(F_t.*cos(theta) - F_mH, F_t.*sin(theta) + F_mV -m2(3).*g,...
F_t.*(H_a(3) - y(3)) + F_mH.*(y(3).*cos(theta) - 0.5.*d1.*sin(theta)...
```

```
) - F_mV.*(y(3).*sin(theta) + 0.5.*d1.*cos(theta)), F_mH - F_bH,...
F_bV - F_mV - m1(3).*g, F_mH.*((H_b(3) - a(3)).*cos(theta) + 0.5.*...
d1.*sin(theta)) + F_bV.*((0.5.*d2 - a(3).*sin(theta)).*cos(theta)) +...
F_bH.*(a(3).*cos(theta) + (0.5.*d2 - a(3).*sin(theta)).*sin(theta))...
- F_mV.*((H_b(3) - a(3)).*sin(theta) - 0.5.*d1.*cos(theta)));
S4 = solve(F_t.*cos(theta) - F_mH, F_t.*sin(theta) + F_mV -m2(4).*g,...
F_t.*(H_a(4) - y(4)) + F_mH.*(y(4).*cos(theta) - 0.5.*d1.*sin(theta)...
) - F_mV.*(y(4).*sin(theta) + 0.5.*d1.*cos(theta)), F_mH - F_bH,...
F_bV - F_mV - m1(4).*g, F_mH.*((H_b(4) - a(4)).*cos(theta) + 0.5.*...
d1.*sin(theta)) + F_bV.*((0.5.*d2 - a(4).*sin(theta)).*cos(theta)) +...
F_bH.*(a(4).*cos(theta) + (0.5.*d2 - a(4).*sin(theta)).*sin(theta))...
- F_mV.*((H_b(4) - a(4)).*sin(theta) - 0.5.*d1.*cos(theta)));

S1 = [S1.F_t, S1.theta, S1.F_mH, S1.F_mV, S1.F_bH, S1.F_bV];
S2 = [S2.F_t, S2.theta, S2.F_mH, S2.F_mV, S2.F_bH, S2.F_bV];
S3 = [S3.F_t, S3.theta, S3.F_mH, S3.F_mV, S3.F_bH, S3.F_bV];
S4 = [S4.F_t, S4.theta, S4.F_mH, S4.F_mV, S4.F_bH, S4.F_bV];

theta1 = 57.2958*S1(2);
theta2 = 57.2958*S2(2);
theta3 = 57.2958*S3(2);
theta4 = 57.2958*S4(2);

% angle from vertical
angle1 = 90 - theta1
angle2 = 90 - theta2
angle3 = 90 - theta3
angle4 = 90 - theta4

% horizontal accelerations
a1 = g*tan(1.5708 – S1(2))
a2 = g*tan(1.5708 – S2(2))
a3 = g*tan(1.5708 – S3(2))
a4 = g*tan(1.5708 – S4(2))
```